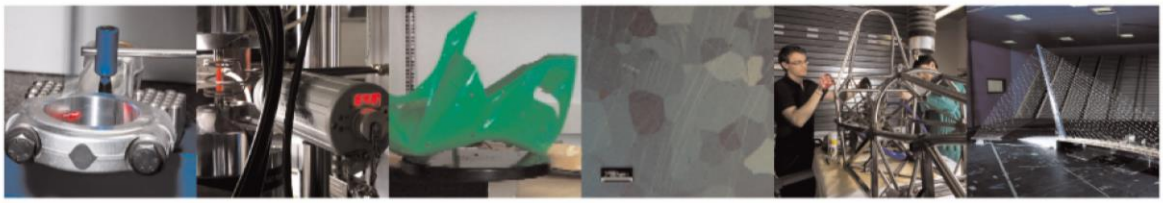

Cooled pads with bioinspired gyroid lattice for tilting pad journal bearings: Experimental validation of numerical model for heat transfer

Dassi, Ludovico; Chatterton, Steven; Parenti, Paolo; Vania, Andrea; Colosimo, Bianca Maria; Pennacchi, Paolo

This is a post-peer-review, pre-copyedit version of an article published in TRIBOLOGY INTERNATIONAL. The final authenticated version is available online at: http://dx.doi.org/10.1016/j.triboint.2023.108448

Cooled pads with bioinspired gyroid lattice for Tilting Pad Journal Bearings: eExperimental validation of numerical model for heat transfer

Ludovico Dassi, Steven Chatterton, Paolo Parenti,
Andrea Vania, Bianca Maria Colosimo, Paolo Pennacchi
Department of Mechanical Engineering, Politecnico di Milano, Via La Masa 1, 20156 Milan, Italy

Abstract

Hydrodynamic journal bearings are essential components for industrial rotating machineries. Continuously growing specific power allows more compact and efficient machines to be obtained, by reducing the environmental footprint of production plants. The aim of this work is to provide a new design of an innovative pad for Tilting Pad Journal Bearings (TPJBs) with an embedded cooling circuit, able to limit the oil film temperature. As a result, specific load can be increased leading to a possible downsizing of the bearing and reduction of lubricant quantity. The heat exchange in the cooling circuit of the pad has been enhanced using bioinspired gyroid lattice. The complete thermo-mechanical study of the pad has been performed with both numerical and experimental analysis. The resulting thermal and mechanical performances have been calculated and discussed. The tested components have been manufactured in stainless steel by using a metal 3D printing technology, based on polymer-metal feedstock extrusion. A performance analysis is conducted to catch differences between the nominal and the printed geometry. The prototype is able to dissipate the generated heat with a higher efficiency, and the pressure drop inside the cooling circuit can be estimated with the numerical model here proposed.

Key-words: Journal bearings, gyroid lattice, Bound Metal Deposition, manufacturability study, internally cooled pads, efficiency.

1 Introduction

Hydrodynamic journal bearings are standard equipment for supporting shaft lines in turbomachines. This technology provides many advantages such as higher load capacity, lower frictional losses and lower maintenance cost than rolling element bearings, which in any case could not be used at all due to peripheral speed and load limitations. . Moreover, the well-known

instability issue of cylindrical hydrodynamic bearings can be faced by adopting a tilting pad layout to make the system stable even at high rotational speeds.

Nowadays, the recent machine design and energy trends require an increase of specific power in production plans and ~~a~~ fast start up procedures. This approach increases the efficiency of the machines but it asks for a more demanding design of the components, including the bearings [1]. Vibrations due to non-linear behaviour can induce instability issues, as discussed by Kim et al. in [2]. In particular, the operating range of tilting pad journal bearings is strongly influenced by the thermal distribution of the sliding surfaces, which results in a thermal pad deformation and in a distorted pressure distribution, as ~~discussed~~ studied by Fillon in [3]. Then, an excessive heating of the component, due to the frictional losses in the oil film wedge, is the main limitation to increase the load capacity, to reduce the coating wear and failures occurrences. In particular fatigue is an important issue for the sliding surfaces of the bearing, as studied by Dong et al. about cavitation phenomena [4] and Yang et al. about the fluttering condition of the upper pads [5].

In the last years, many research activities have tried to implement an active temperature control by proposing different layout solutions. For example the oil mass flow from the jacking pump circuit can be tuned in order to modify the dynamic characteristics of the bearing [6] [7]. Moreover, new design solutions, like leading edge groove, have increased the cooling capacities and they have reduced the oil consumption. This layout has been deeply investigated by many authors, such as Hagerman et al. [8] and Abdollahi et al. [9]. The reduction of oil temperature is accomplished by increasing the turbulence intensity [10] and by implementing an active control on the delivered oil quantity ~~delivered~~ [11].

Schuler et al. [12] further improve the oil cooling by ~~exploiting~~exploiting the effect of turbulence generated by eddy grooves, or Yang et al. in [13] implement a power loss reduction technique by favouring oil cavitation. By inserting a pocket and step feature in the pads, it is possible to reduce the power losses up to 27% with beneficial effects on maximum speed and surface temperature.

The internal cooling of pads, by using a dedicated circuit, is a promising arrangement to properly cool down pads. Starting from 2014, Najar and Harmain [14] have proposed and quantified the advantages of using a water-cooling circuit with different channel shapes (M-shaped or bifurcated path) for a thrust bearing pad, studying and updating the geometry in another paper [15]. In this last manuscript the theorical analysis is carried out by a numerical model to predict the temperature distribution into the pad. The most relevant outcome is that the cooling circuit can remove up to 30% of the thermal power generated by the oil friction.

ha formattato: Tipo di carattere: Non Corsivo

ha formattato: Francese (Francia)

ha formattato: Francese (Francia)

Codice campo modificato

ha formattato: Francese (Francia)

ha formattato: Francese (Francia)

Codice campo modificato

ha formattato: Tipo di carattere: Non Corsivo, Francese (Francia)

ha formattato: Francese (Francia)

ha formattato: Francese (Francia)

ha formattato: Francese (Francia)

Codice campo modificato

ha formattato: Tipo di carattere: Non Corsivo

To overcome the production complexities of the cooling circuit, Additive Manufacturing (AM) technologies can be used. Chatterton et al. in [16] address this topic, by considering a journal bearing and a cooled pad with an M-shaped channel. Firstly, they created an advanced ~~full~~ Thermo-Elastic-Hydro-Dynamic model to compare the performances of different channel cross sections and then they made a functional prototype of the component~~,~~ [17]. The best results are obtained by using a 6-square-multichannel arrangement as cross section of the cooling circuit. The results show that the average surface temperature is significantly reduced with respect to the same pad without internal cooling circuit. The numerical model has also been validated by an experimental campaign.

An innovative way to further improve the dissipated heat from the cooling circuit is to increase the exchanging area and to sustain vorticity in the coolant. The evolution of metal 3D printing technologies allows increased geometrical freedom, therefore complex internal structures can be shaped inside the pad to accomplish this task. For instance, gyroid lattice is a bioinspired innovative geometry with relevant heat exchange properties, as discussed by Kaur et al. in [18]. As reported by in Li et al. in [19], gyroid lattice has been discovered by the NASA physicist Alan Schoen in 1970s, by studying the nanoscale biological microstructures of C. Ruby species butterflies by using a Scanning Electron Microscope (SEM). It has been found that wing microstructure is organized in complex and hierarchical structures on different length scales to realize different functions and to adapt to natural environments. The main surfaces are covered by inter-connected ridges and ribs, providing mechanical stability, and serving as interference reflectors to dump external forced vibrations.

The basic idea of this paper is to take advantage of metal 3D printing technology to design complex geometries which can enhance the heat transfer performances by means of an increased heat transfer contact area and compactness [20]. As a result, heat exchangers of new generation, called Printed Circuit Heat Exchangers (PCHE), can be design and manufactured. Thanks to their small overall dimensions, lightweight structures, and improved high heat transfer efficiency they can find many innovative application fields, ~~like the~~such as CO2 supercritical Rankine cycles [21]. Among the available lattice structures, that can be found in the literature, only gyroid lattices have been investigated in this paper. The main advantages of such lattices are the increase of the exchanging surfaces, the possible onset of turbulent condition and the continuous rounded shape without sharp edges which is beneficial for the mechanical resistance. Thus the channel can contribute supporting the load.~~.~~

ha formattato: Tipo di carattere: Non Corsivo

The aim of this manuscript is to provide a preliminary ~~a full~~ thermo-mechanical design of a cooled pad with a conformal cooling circuit based on gyroid lattice. Both oil ISOVG68 and water are considered as coolant fluids, while the pad is made of stainless steel SS316L with a white metal SbSn8Cu4 lining. Numerical simulations were performed for a proper selection of the lattice design parameters. The structural behaviour was estimated by *Finite Element* ~~*Modeling*~~*Modelling* (FEM) analysis while the heat exchanged and internal fluid dynamics of the coolant by *Computational Fluid Dynamics* (CFD). A discussion on the simplification hypothesis and modelling schemes of the complex internal geometry are included. Pad geometry design is addressed by taking into account the requirements of the functional component, as well as the technological constraints given by the adopted AM process. After building the prototypes, experimental flushing has been performed to ~~validate~~ catch differences between the printed geometry and the nominal one considered in the fluid-dynamic model~~, which is useful in the design phase.~~.

2 Gyroid Lattice structures

~~2~~2.1 Analytical definition

From the analytical point of view, the g~~G~~yroid is formalized as a Triple Period Minimal Surface (TPMS) geometry [22]. The surface is defined as minimal, when it locally minimizes its surface energy given a certain boundary. As a result, it has smooth curvatures with no edges or corners. TPMS geometries without self-intersections divide the domain into two disjoint and intertwining domains, which are simultaneously continuous. The level-set approximation technique is used to obtain TPMS lattices, which have cubic symmetry and they are periodic in the three-dimensional space. The fundamental equation of minimal surface for ~~ga G~~yroid is ~~as follows~~reported here:

$$\phi(x, y, z) = \cos(x)\sin(y) + \cos(y)\sin(z) + \cos(z)\sin(x) = 0 \quad (1)$$

where x, y, z are cartesian coordinates.

Once the minimal surface is defined, there are two possible ways to create gyroid structures. The first one relies on the surface thickening and brings to sheet based TPMS structures. The surfaces facing towards the individual domains are offset in two directions perpendicular to the surface, creating a solid ~~surface~~ wall with a homogeneous thickness (Figure 1~~Figure 1~~~~Figure 1~~a). The second way is obtained by solidifying one of the two volumes defined by the minimal surface, yielding to a skeletal based TPMS structure (Figure 1~~Figure 1~~~~Figure 1~~b).

ha formattato: Inglese (Regno Unito)

ha formattato: Inglese (Regno Unito)

Formattato: Titolo 2, Rientro: Sinistro: 0 cm, Sporgente 1.02 cm, SpazioPrima: 6 pt

ha formattato: Tipo di carattere: Non Grassetto

ha formattato: Tipo di carattere: Non Grassetto

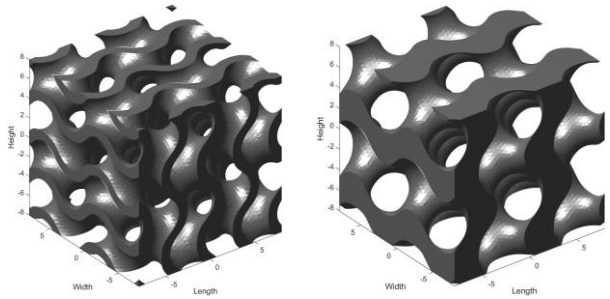

(a) (b)

Figure 1. *Gyroid lattice 3D models:* ***(a)*** *sheet based,* ***(b)*** *skeletal based.*

The relevant parameters which have to be set to fully define the gyroid lattice shape are: the lattice type (sheet or skeletal), the unit cell length (edge of the minimum repeatable cell), the relative density (percentage of solid volume in an elementary cube) and the external lattice dimensions (obtained by repetition in space of the minimum cell).

2.2 Heat exchange properties

The gyroid lattice can guarantee relevant performances for TPJB application. According to Li et al. studies [19], also confirmed by several other authors like Koneri et al. [23] and Zhang et al. [24], gyroid lattice figures out the best heat ~~transfer~~transfer rate with respect to the other open cell periodic lattices. The authors considered a simple cylindrical pipe used as a representative section of a heat exchanger, water is used as coolant and the temperature of the outer shell is imposed. The pipe is then filled with a selection of the more promising lattices (i.e. gyroid, Star Kogeme and Cubic body centred). The comparison is conducted by considering the pressure drop needed for the circulation of a specified coolant flow rate and the heat transfer rate between the coolant and the outer shell, as shown in Figure 2.

Formattato: Didascalia, Allineato a sinistra, Rientro: Prima riga: 0 cm, Interlinea: singola

Formattato: Titolo 2, Allineato a sinistra, Rientro: Sinistro: 0 cm, Sporgente 1.02 cm, SpazioPrima: 6 pt, Dopo: 6 pt, Interlinea: singola

ha formattato: Francese (Francia)

ha formattato: Francese (Francia)

ha formattato: Francese (Francia)

ha formattato: Francese (Francia)

ha formattato: Tipo di carattere: Non Corsivo

ha formattato: Tipo di carattere: Non Corsivo

ha formattato: Tipo di carattere: Non Grassetto, Non Corsivo

Codice campo modificato

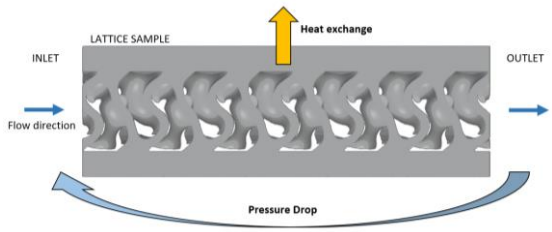

Figure 2*. Schematic representation of the thermal-fluid quantities of interest.*

From the results, gyroid lattice figures out the highest values of both the two variables with respect to the other lattices. The heat exchange can be increased of 50-60% with a higher pressure drop +500% as drawback. The Overall Enhancement Factor (OEF) is a suitable indicator to effectively quantify the increase of heat exchange with respect to the pressure increase [23]. The definition of the OEF is reported in the following expression:

$$OEF = \frac{Q/Q_0}{\Delta P/\Delta P_0} \qquad (2)$$

where Q and ΔP are the heat exchange and the pressure drop of the considered lattice while Q_0 and ΔP_0 are the same quantities referred to a plain cylindrical pipe. According to the authors, the OEF of the gyroid lattice is 3 times higher than other lattices.

For practical design criteria, since the heat transfer power is some order of magnitude higher than the required hydraulic power, it is a common practice to simply limit the pressure drop to a desired value, convenient for the application. So that, the increased heat exchange becomes the most relevant quantity to be maximized.

2.3 ~~[23]like Schwarz-D or diamond ones.~~ Mechanical properties

The gyroid lattice features ~~Moreover, the lattice has got~~ relevant mechanical properties for its lightweight. Al-Ketan et al. [25] intensively studied the mechanical resistance and stiffness of ~~the~~ several lattices with respect to the bulk material, under the hypothesis of periodical structure and linear deformations. ~~and they compared different lattice geometries.~~ By ~~performing some numerical analysis~~ considering the dominant deformation modes of the unit cell, the authors justified the higher structural efficiency ~~the better mechanical properties~~ of the gyroid lattice by ~~considering that gyroid lattice~~noticing that ~~promotes~~ tensional axial stresses are promoted inside the thin walls, while other lattices (i.e. diamond and octet truss) are dominated by bending modes. ~~-~~

Formattato: Allineato al centro, Mantieni con il successivo

ha formattato: Tipo di carattere: Non Grassetto

Formattato: Allineato al centro

Formattato: Titolo 2, Allineato a sinistra, Rientro: Sinistro: 0 cm, Sporgente 1.02 cm, SpazioPrima: 6 pt, Dopo: 6 pt, Interlinea: singola

This fact increases the gyroid lattice stiffness and, consequently, the relative Young modulus generally reaches 5% with respect to the bulk material and the ultimate strength around 10%.

2.4 Printability

Due to the high complexity of pad internal geometry, the most suitable technology for the production is metal AM, a technology that allows producing 3D functional prototypes in metal with a near-net-shape output, as presented in [26]. In particular, material extrusion Metal 3D printing technology, i.e. the Bound Metal Deposition® (BMD) system, is chosen for its advantages. The production route is composed by three main steps which are: the printing of the feedstock at low temperature (around 180 °C), debinding from polymeric binder and sintering in an electric furnace (around 1360°C for the adopted stainless steel SS316L). One of the key advantages is that, after printing, there is no resulting powder to be flushed away from internal cavities, which may be a difficult operation for a complex shaped channel. Moreover, this technology is flexible as it is successful in handling a wide range of materials, including copper, which is a promising pad development. Furthermore, this technological solution reaches high dimensional-geometrical precision [27], reducing printing defects and porosity issues, which are detrimental for the mechanical properties of the pad.

3 Design of pad geometry

33.1 Preliminary design choices

The considered bearing is a five-pad TPJB with nominal shaft diameter of 100 mm. The most relevant data of the bearing are listed in Table 1~~Table 1~~Table 1. The geometry layout is a rocker-back pivot in load-on-pad configuration (LOP), as shown in Figure 3~~Figure 3~~Figure 2a. The pressure and the temperature distributions are calculated by means of a bearing model, fully described by the same authors in some previous articles, such as [28] and [29]. The resulting plots are shown in Figure 3~~Figure 3~~Figure 2b-3~~2~~c and they are used as input for the current analysis. For the sake of simplicity, the temperature field is reduced to a uniform distribution equal to the mean value (60°C).

Formattato: Titolo 2, Allineato a sinistra, Rientro: Sinistro: 0 cm, Sporgente 1.02 cm, SpazioPrima: 6 pt, Dopo: 6 pt, Interlinea: singola

Formattato: Rientro: Prima riga: 0 cm

Formattato: Titolo 2, Rientro: Sinistro: 0 cm, Sporgente 1.02 cm, SpazioPrima: 6 pt

ha formattato: Tipo di carattere: Non Grassetto, Colore carattere: Automatico

ha formattato: Tipo di carattere: Non Grassetto

ha formattato: Tipo di carattere: Non Grassetto, Non Corsivo, Controllo ortografia e grammatica

ha formattato: Tipo di carattere: Non Grassetto

ha formattato: Tipo di carattere: Non Grassetto, Non Corsivo, Controllo ortografia e grammatica

***Table 1**. Bearing data.*

Shaft diameter [mm]	100
Pad outer radius [mm]	59.60
Pad length [mm]	70
Assembled clearance [µm]	60
Machined clearance [µm]	130
Pad span angle	60°
Total pad thickness [mm]	16
Lubricant	Oil ISOVG68
Oil flow rate [L/min]	2
Load [KN]	5
Speed [rpm]	3000

Tabella formattata

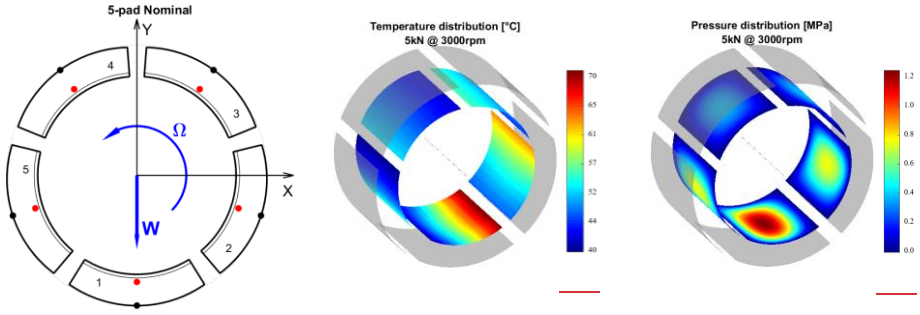

(a) (b) (c)

***Figure 3~~2~~**. **(a)** Bearing assembly sketch, **(b)** temperature distribution and **(c)** pressure distribution.*

ha formattato: Tipo di carattere: Corsivo

ha formattato: Tipo di carattere: Corsivo

Codice campo modificato

The journal bearing is composed of~~by~~ five flooded lubricated pads, and only the bottom one, the more loaded, is assumed to be internally cooled, whereas the optimal solution is represented by all cooled pads. The baseline cooling arrangement is composed ~~by~~of an M-shaped circuit characterized by 6-squared channels cross section, as shown in Figure 4~~Figure 4~~~~Figure 3~~a. The baseline design is the same already investigated by the same authors in [16] and manufactured by Selective Laser Melting (SLM) process. The outer dimensions of the pad are kept constant and only the internal cooling circuit is changed in the new proposed solution. For a successful design, both mechanical and thermal aspects must be considered. On the one hand, the gyroid lattice should increase the maximum heat exchange, but on the other hand it should not negatively impact on the

ha formattato: Tipo di carattere: Non Grassetto

actual mechanical stiffness of the 6-channels pad. First of all, two possible new designs for the internal layout have been investigated with respect to the baseline. The first design is to keep the M-shaped channel and fill it with gyroid lattice (Figure 4~~Figure 4~~~~Figure 3~~b), choosing accurately the cross-sectional area and the lattice parameters to balance the performances. The second one is a cross flow heat exchanger that can be created with two parallel channels and a diffused gyroid lattice in the central portion of the pad internal volume, as shown in Figure 4~~Figure 4~~~~Figure 3~~c.

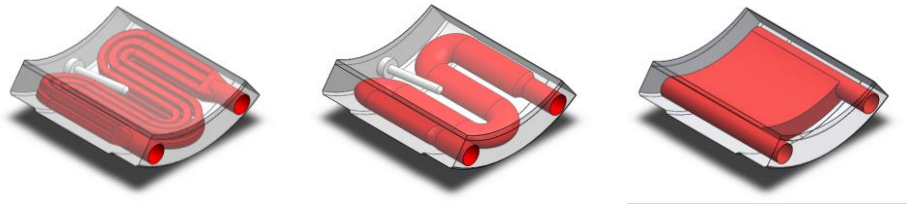

(a) (b) ~~(c)~~(c)

Figure ~~44~~3. (a) *Baseline solution,* ***(b)*** *M-shape-path filled with gyroid,* ~~,~~***(c)*** ~~*new designs filled with gyroid lattice*~~*diffused gyroid lattice*.

The last layout has been disregarded due to its lack in mechanical stiffness, while being interesting for the larger internal volume and the relevantly improved thermal properties. From the literature data on TPMS lattices [30], the maximum compression stiffness is, in fact, 5% of the bulk material and it is considered not enough for pad application. The resulting compliances would affect the oil film wedge and shaft line dynamics with unpredictable effects, so M-shaped layout has been chosen in this study.

3.2 Internal lattice choice

To facilitate the comparison with the baseline layout, the net cross-sectional area available to the fluid, has been kept equal to the original amount, i.e. 50 mm^2. By considering an internal filling with lattice geometries and choosing a percentual available area of 67%, the channel total section area is calculated as 75 mm^2. An elliptical duct (8 mm x 12 mm vertical and horizontal main axis respectively) guarantees the area and correctly fits with pad dimensions; in addition, round edges avoid stress intensification, and assure better printability of the component.

In this regard, ~~to guarantee the printability,~~ cell length is chosen to be 8mm to guarantee the printability, while the lattice type is arbitrary and the relative density should range in the interval 20-50%. Since the scientific literature is still ~~lacking~~ incomplete in comparing~~-~~ the performances of

ha formattato: Tipo di carattere: Non Grassetto, Colore carattere: Automatico

ha formattato: Tipo di carattere: Non Grassetto

ha formattato: Tipo di carattere: Non Grassetto

ha formattato: Tipo di carattere: Non Grassetto

Formattato: Titolo 2, Allineato a sinistra, Rientro: Sinistro: 0 cm, Sporgente 1.02 cm, SpazioPrima: 6 pt, Dopo: 6 pt, Interlinea: singola

~~TPMS~~ different gyroid lattices geometr~~y~~ies, a preliminary study is here performed to define the ~~gyroid lattice~~set of parameters with mechanical a~~nd the~~ thermo~~rmo~~-fluid dynamics performance best fitting to the given application.

The fluid-~~-~~dynamics performances of the lattice are here investigated carrying out both numerical and experimental tests. Simple cylindrical samples, i.e. "tubes", manufactured in stainless steel SS316L and filled with different gyroid lattices, are considered to mimic the functioning of the final pad, whilst simplifying the numerical and experimental investigations. In particular, a ~~complete~~ thermo-fluid dynamics analysis is performed to find the best trade off on performances (pressure drop and heat exchange) for pad application. The considered tubes are 50 mm long (1/4 of the total length of the pad cooling circuit), while the cross-sectional area is equivalent to the one of the baseline pad geometry. The analysis has been performed to directly match the different lattice geometries and to study the effects of the parameters settings (cell length, relative density, working fluid~~, flow rate and solid material~~) on the fluid dynamic properties of interest~~(pressure drop and heat exchange)~~. Therefore, six lattice layouts are selected for the analysis by changing the lattice type and the relative density; namely densities 35, 45% for sheet structure and densities 12, 25, 35, 45% for solid structure as reported in Table 2. Sheet lattices with lower relative density are not considered because they face relevant printing problems with BMD technology.

***Table 2**. Types of gyroid lattices for filling of tubes.*

Type \ *Density*	15%	25%	35%	45%
Sheet	✘	✘	✓	✓
Solid	✓	✓	✓	✓

The types of the boundary conditions have been chosen similarly to the existing ones in the literature [23] while the values are chosen for the application, in particular a flow rate of 6L/min and inlet temperature of 40°C are assigned for the coolant while temperature of the outer wall of the tube is imposed to 60°C. Both oil ISOVG68 and water are analysed. ~~-~~Mesh sensitivity analysis and experimental validation are performed to validate the numerical model on the pressure drop with errors lower than 5%.~~-~~ An example of the computed pressure and temperature fields from the numerical analysis ~~tubes~~ are shown in Figure 5a and Figure 5b while a printed tube is shown in Figure 5c.

~~considered for its preliminary study is shown in Figure 4.~~

ha formattato: Tipo di carattere: Non Grassetto
Codice campo modificato
ha formattato: Pedice
ha formattato: Apice
Tabella formattata
ha formattato: Tipo di carattere: (Predefinito) MS Shell Dlg 2, Italiano (Italia)
ha formattato: Tipo di carattere: (Predefinito) MS Shell Dlg 2, Italiano (Italia)
Formattato: SpazioPrima: 0 pt, Dopo: 0 pt, Non mantenere con successivo, Sillabare, Non regolare lo spazio tra testo asiatico e in alfabeto latino
Formattato: SpazioPrima: 0 pt, Dopo: 0 pt, Non mantenere con successivo, Sillabare, Non regolare lo spazio tra testo asiatico e in alfabeto latino
Formattato: Rientro: Prima riga: 0 cm
Formattato: Giustificato
ha formattato: Non Evidenziato
ha formattato: Tipo di carattere: Non Grassetto, Non Corsivo
Codice campo modificato
ha formattato: Non Evidenziato

(a)

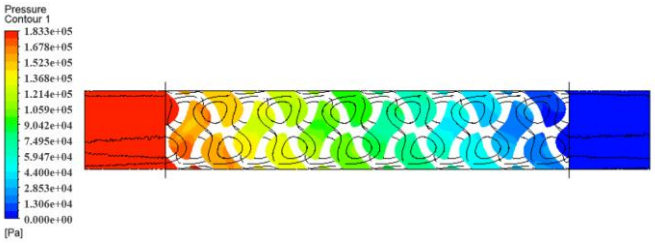

(b)

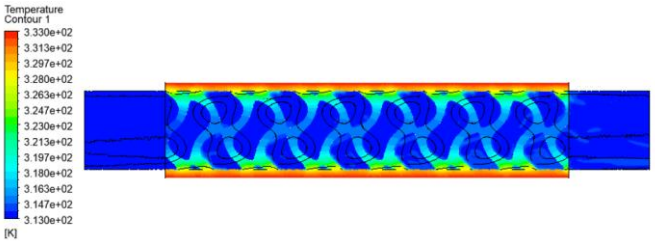

(c)

~~*This analysis is not reported here for the sake of brevity. Finally, gyroid lattice with sheet layout and relative density RD=35%, named "sheet 35%" in the following, is chosen. An example of the tubes considered for its preliminary study is shown in Figure 4.*~~

Figure ~~5~~4. *Analysis of tube filled with "sheet 35%" lattice: numerical results of pressure **(a)** and temperature **(b)** fields; ~~F~~functional prototype "sheet 35%" tube **(c)** for preliminary study.*

ha formattato: Tipo di carattere: Corsivo

Formattato: Allineato al centro, Rientro: Prima riga: 0 cm

ha formattato: Tipo di carattere: Corsivo

Formattato: Rientro: Prima riga: 0 cm

ha formattato: Tipo di carattere: Non Grassetto, Corsivo

ha formattato: Tipo di carattere: Corsivo

ha formattato: Tipo di carattere: Non Grassetto, Corsivo

ha formattato: Tipo di carattere: Corsivo

ha formattato: Tipo di carattere: Non Grassetto, Corsivo

ha formattato: Tipo di carattere: Corsivo

ha formattato: Tipo di carattere: Non Grassetto, Corsivo

Formattato: Normale, Allineato al centro, Interlinea: 1.5 righe, Mantieni con il successivo

ha formattato: Tipo di carattere: Corsivo

ha formattato: Tipo di carattere: Grassetto, Corsivo

ha formattato: Tipo di carattere: Corsivo

ha formattato: Tipo di carattere: Non Grassetto, Corsivo

ha formattato: Tipo di carattere: Corsivo, Non Evidenziato

ha formattato: Tipo di carattere: Corsivo

ha formattato: Tipo di carattere: Corsivo, Non Evidenziato

ha formattato: Tipo di carattere: Grassetto, Corsivo, Non Evidenziato

ha formattato: Tipo di carattere: Corsivo

ha formattato: Tipo di carattere: Corsivo

ha formattato: Tipo di carattere: (Predefinito) Calibri, 11 pt

Formattato: Normale

The main goal of this analysis is to increase as much as possible the heat transfer between the outer tube shell and the flowing coolant, while taking into account the increase of back pressure for the coolant, by considering the OEF index. From the results, sheet lattice has a higher heat exchange performance compared to the solid one (Figure 6a) probably because of the more finned lattice structure, so it is preferred. Then the sheet lattice with RD=35% figures out a higher OEF with respect to RD=45% (Figure 6b). The OEF factor is calculated according to Equation 2, by considering the heat exchange and counterpressure values calculated for each lattice. A higher OEF is favourable because it means a lower pressure drop for the fluid. These considerations are valid both for oil and water as coolant but water figures out a three times higher heat exchange values. The full analysis on the tubes samples not reported here for the sake of brevity. Finally, gyroid lattice with sheet layout and relative density RD=35%, named "sheet 35%" in the following, is chosen for the pad application.

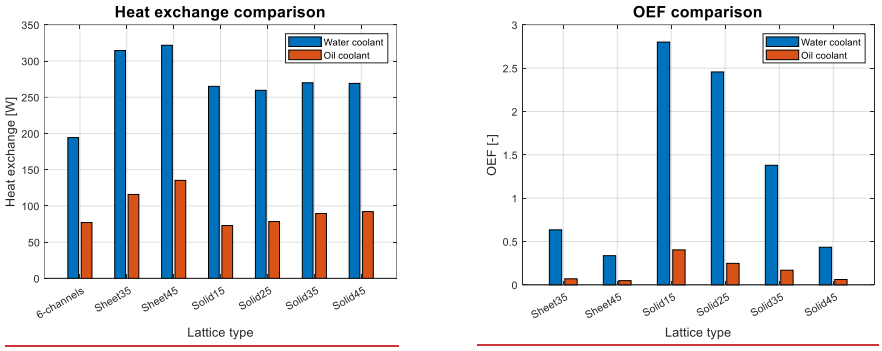

(a) (b)

Figure 6. *Comparative analysis on gyroid lattices with flow rate 6L/min; Maximum exchangeable heat* ***(a)****, Overall Enhancement Factor* ***(b)****.*

3.3 Pad design for a successful manufacturing

The ~~building~~ manufacturing with the AM process requires geometrical corrections to provide the successful production of the pads. Common rules for AM design have been considered, in terms of printing tolerances, maximum overhang angles and supported structures, part sintering stability, maximum aspect ratio and filament stringing issue. Then, a metal stock of 1 mm is added over all surfaces for enabling subsequent mechanical finishing operations by milling process. The addition

ha formattato: Non Evidenziato

ha formattato: Non Evidenziato

ha formattato: Non Evidenziato

ha formattato: Non Evidenziato

ha formattato: Non Evidenziato

ha formattato: Non Evidenziato

ha formattato: Non Evidenziato

ha formattato: Tipo di carattere: Grassetto, Non Evidenziato

ha formattato: Non Evidenziato

ha formattato: Tipo di carattere: Grassetto, Non Evidenziato

ha formattato: Tipo di carattere: (Predefinito) Calibri, 11 pt

Formattato: Allineato a sinistra, Rientro: Prima riga: 0 cm, SpazioDopo: 8 pt, Interlinea: singola

of local lattice piercings and venting holes, shown in Figure 7~~Figure 7~~~~Figure 5~~, are useful to speed up the production time during the debinding phase. Moreover, lattice piercings help to balance the pressure between the two fluid domains of gyroid lattice, in particular near channels curves. An example of the unbalanced pressure field is shown in Figure 14~~Figure 14~~~~Figure 11~~, where piercings are intentionally not present.

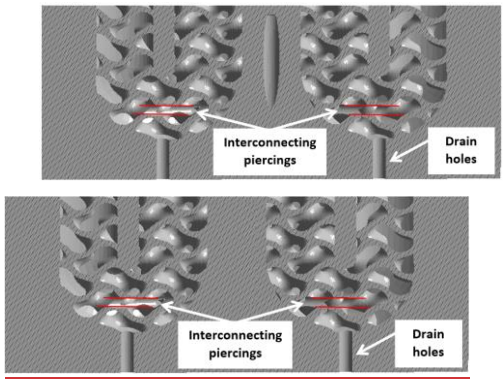

Figure ~~7~~7~~5~~. *Details of internal channel design: lattice piercings and drain holes.*

The pad is printed in stainless steel SS316L, with vertical orientation in two specimens by varying the printing orientation angle. Delamination issues arise with horizontal layering while a 20° pad tilting avoids this issue. It is also relevant to consider that the surface roughness changes, depending on the layering orientation. The pad printed with vertical orientation, labelled as pad #1, has a surface roughness of Ra=16 µm while the pad printed with an orientation of 20°, labelled as pad #2, has a roughness of Ra=22 µm. This aspect is properly measured with an optical 3D microscope ~~type~~ (Brucker Alicona G4) since it will affect the internal fluid dynamics of the coolant. Finally, only pad #2 is coated with Babbitt (white metal), and it is mechanically finished in all the surfaces ~~to~~ making~~e~~ it ready for the final application. The prototype of pad #2 is shown in Figure 8~~Figure 8~~~~Figure 6~~a-7~~6~~b, while pad #1 is rejected due to leakage and delamination issues. Actually, pad #1~~it~~ has ~~only~~ been only used for comparative analysis on pressure drop. A visual inspection of the internal channel for the pad #2 is shown in Figure 8~~Figure 8~~~~Figure 6~~c.

ha formattato: Tipo di carattere: Non Grassetto

ha formattato: Non Evidenziato

Formattato: SpazioDopo: 8 pt

ha formattato: Tipo di carattere: (Predefinito) Calibri, 11 pt

Formattato: Normale

Formattato: Titolo 2, Rientro: Sinistro: 0 cm, Sporgente 1.02 cm, SpazioPrima: 6 pt, Dopo: 6 pt

ha formattato: Tipo di carattere: Non Grassetto

ha formattato: Tipo di carattere: Non Grassetto

(a) (b) (c)

Figure 8~~6~~. *Functional prototype of pad #2 as printed* ***(a)*** *and coated and milled* ***(b)****, inspection of internal channels.*

Formattato: Didascalia

4 Pad deformation

4.1 FEM simulation setup

The pad is, at first, a structural element of the bearing, therefore a ~~F~~finite e~~E~~lements static structural analysis has been performed to calculate static deformations of "sheet 35%" lattice and other type of lattices. The purpose of this analysis is to compare the static deformation of the component depending on the internal lattice type, where the effect of temperature is here neglected. A FE~~M~~ model of the pad is generated considering the complex lattice geometry adopted and Babbitt alloy coating on the top surface. The material properties are listed in Table 3~~Table 3~~~~Table 2~~. Stainless steel SS316L and standard Babbitt alloy SnSb8Cu4 have been assumed for the base part and the lining of the pad, respectively.

ha formattato: Tipo di carattere: Non Grassetto, Non Corsivo, Colore carattere: Automatico

ha formattato: Tipo di carattere: Non Grassetto, Colore carattere: Automatico, Controllo ortografia e grammatica

Table 3~~3~~*. Materials mechanical properties.*

	Base part	***Lining***
Material	SS316L	SnSb8Cu4
Mass density [kg/m^3]	8030	7300
Young modulus [GPa]	200	53
Poisson ratio	0.3	0.35
Compressive Yield Strength [MPa]	300	89
Tensile Yield Strength [MPa]	300	80

ha formattato: Tipo di carattere: Corsivo

ha formattato: Tipo di carattere: Corsivo

ha formattato: Tipo di carattere: Corsivo

ha formattato: Tipo di carattere: Corsivo

ha formattato: Tipo di carattere: Grassetto

Tabella formattata

ha formattato: Tipo di carattere: Non Corsivo

The FEM simulations have been performed with the same external loading conditions in [29]. The pressure distribution to be applied to the pad surface is shown in Figure 3~~Figure 3~~Figure 2c. Geometry is clamped in the pivot region along an artificial strip surface; this allows simplifying the case, avoiding the implementation of a contact model, even if this boundary condition causes some localized stress intensification in the bottom surface, which is ~~in any case~~not of interest for this part of the proposed study. To simplify the analysis, the effect of thermal expansion is neglected at this phase and only the effect of the static load is considered. So, no temperature effects have been considered in this analysis. A tetrahedral mesh is used to adapt cells to complicate lattice geometry and mesh sensitivity analysis is performed.

ha formattato: Tipo di carattere: Non Grassetto, Colore carattere: Automatico

ha formattato: Tipo di carattere: Non Grassetto, Non Corsivo, Colore carattere: Automatico, Controllo ortografia e grammatica

4.2 FEM results analysis

The computed Von Mises stress and the pad deformation for the lattice "sheet 35%" are shown in Figure 9~~Figure 9~~Figure 7. The proposed solution guarantees no stress intensification inside the lattice domain and low absolute values of Von Mises stress (40 MPa). This is an important aspect to prevent cracking formation between the printed layers.

ha formattato: Tipo di carattere: Non Grassetto

The maximum deformations of the pad for different lattice structures, as well as their relative deformation with respect to the baseline, are listed in Table 4~~Table 4~~Table 3. Both the lattice type (sheet or solid) and the relative density (15%-45%) are varied. The deformations have been estimated as the maximum vertical deformation of the pad geometry, located in the corner tip of the sliding surface when the nominal load is applied.~~.~~

ha formattato: Tipo di carattere: Non Grassetto, Colore carattere: Automatico

Looking at the results, "sheet 35%" lattice has 11% less deformation than the baseline solution, so gyroid lattice is more beneficial on the load carrying capacity than squared channels. The best result can be obtained with a "sheet 45%" lattice, even if this lattice structure shows an excessively high pressure drop for the cooling circuit~~.~~, so it has not been chosen for the prototypes.

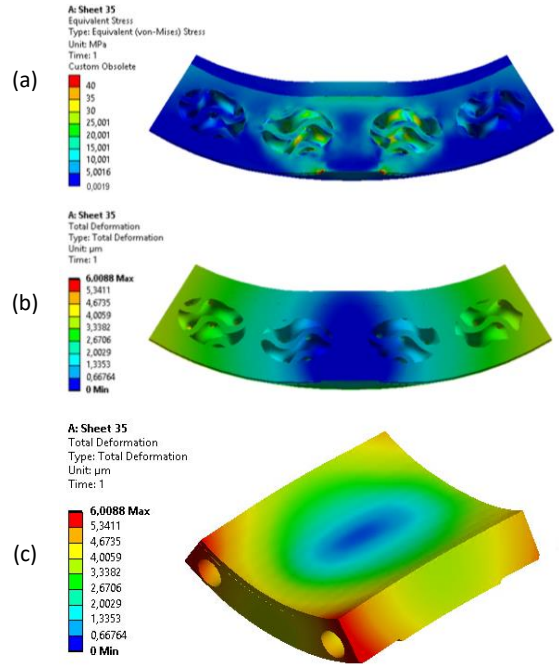

Figure ~~997~~. *Results of static FEM analysis of pad with "sheet 35%" gyroid lattice infill under nominal load:* ***(a)*** *Von Mises stress,* ***(b, c)*** *total deformation.*

Table ~~443~~. *Static deformation for different pad internal infill lattices.*

Internal Layout	***Maximum deformation [µm]***	***Deformation difference [%]***
6-channels	6.77	-
Sheet 35%	6.00	-11.3%
Sheet 45%	4.11	-39.2%
Solid 15%	7.70	+13.7%
Solid 25%	6.85	+1.2%
Solid 35%	6.21	-8.3%
Solid 45%	4.31	-36.4%

ha formattato: Tipo di carattere: Grassetto

Tabella formattata

5 CFD thermo-fluid-dynamic analysis

5.1 CFD simulation setup

A numerical model is used to study the thermal diffusion phenomenon of the pad and internal fluid dynamics. For a generic material element, thermal diffusion is governed by the Fourier-Biot relation, as follows:

$$K \cdot \nabla^2 T = \rho \cdot C \cdot \frac{dT}{dt} - \dot{g} \qquad (23)$$

where *K* is the thermal conductivity coefficient, *T* is the temperature, *ρ* is the material mass density, *C* is the specific thermal capacity and $\dot{g}$ is the source coefficient. This model is valid both in solid and fluid domains, where in the latter also advection term is present in the latter one.

For the pad case study, Navier-Stokes equations are solved to predict the fluid dynamics regime under hypothesis of steady state condition, viscous and incompressible fluid. To consider the turbulence effects, a 2-equations $k-\omega\ SST$ (Shear Stress Transport) model has been used. Actually, it is the most common choice for turbomachinery complex flow calculations, and it is presently considered the standard choice for RANS (Reynolds Average Navier-Stokes equations) calculations in this field of application. The $K-\omega\ SST$ model fully solves boundary layer development under the hypothesis of no slip condition and it requires the check of the *adimensional momentum thickness (y+)* value at the walls. For the simulations, the *firstly walls are considered smooth and then a tuning process on surface roughness parameter (Ra)* of the walls is performed, as discussed in section 7considered and it is imposed to the same values measured with the optical microscope: Ra=16 µm for pad #1 and Ra=22 µm for pad #2. The surface roughness value has possibly relevant effects on the coolant flow since it could increase the resulting pressure drop. The main reason comes from the interaction between the turbulent regime and the micro-peaks of the walls surface; therefore this effect is notable only when water is used and turbulent regime occurs. The numerical model is used also to compare the effect of different materials. Solid domain can be made of steel or copper, while fluid domain can work with water or lubricant oil ISOVG68 [31]; such oil is a common industrial choice for the lubricating circuit of the pad. The same oil can be used for the cooling circuit, avoiding any possible contamination issues between lubrication and cooling fluids. Furthermore, the same supply circuit of the lubrication can be used for the coolant. The material properties are obtained from the literature and listed in Table 5Table 5Table 4. The dependence of oil mass density and dynamic viscosity as a function of the temperature are shown in Figure 10Figure 10Figure 8.

ha formattato: Tipo di carattere: Corsivo
ha formattato: Tipo di carattere: Corsivo
ha formattato: Non Evidenziato
ha formattato: Tipo di carattere: Corsivo, Non Evidenziato
ha formattato: Tipo di carattere: Corsivo
ha formattato: Non Evidenziato
ha formattato: Tipo di carattere: Corsivo, Non Evidenziato
ha formattato: Non Evidenziato
ha formattato: Non Evidenziato
ha formattato: Non Evidenziato
ha formattato: Tipo di carattere: Non Grassetto, Colore carattere: Automatico
ha formattato: Tipo di carattere: Non Grassetto, Colore carattere: Automatico

Table 5~~5~~4. *Materials thermal properties.*

Material	***Density [kg/m³]***	***Dynamic viscosity [Pa·s]***	***Specific Heat [J/kg-K]***	***Thermal conductivity [W/m-K]***
Steel SS316L	8030	-	502	16.27
Copper	8978	-	381	387.60
SnSb8Cu4	7300	-	230	45.00
Water	998	0.001	4182	0.60
Oil ISOVG68 (40°C)	878	0.04	1934	0.15

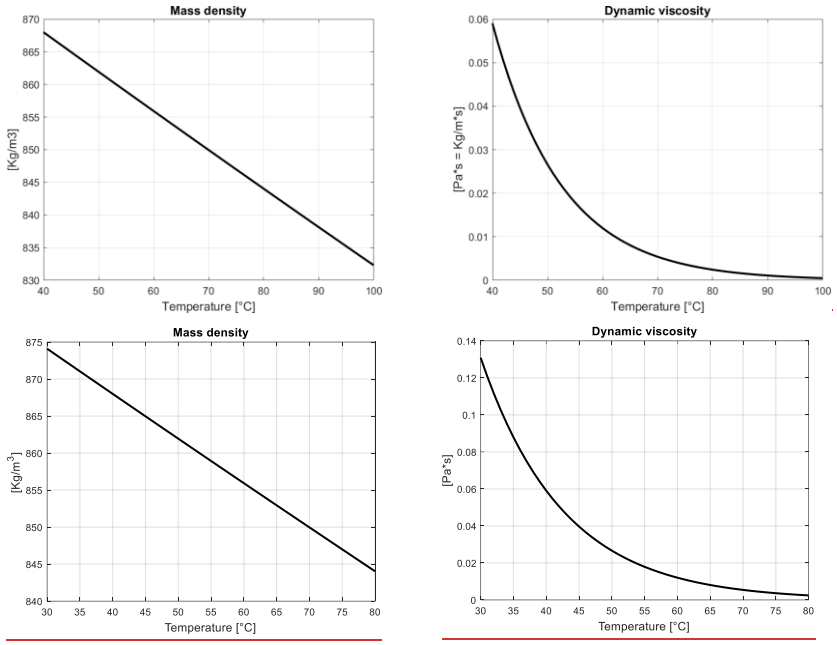

(a) (b)

Figure 10~~10~~8. *Oil ISOVG68 properties as function of temperature:*

(a) *mass density,* ***(b)*** *dynamic viscosity.*

ha formattato: Tipo di carattere: Grassetto

Tabella formattata

Formattato: Allineato a sinistra

5.2 Mesh sensitivity analysis

The simulated geometry is composed by two domains, the solid pad structure and the fluid domain, whose meshes are shown in Figure 11~~Figure 11~~~~Figure 9~~a-1~~0~~b. The total mesh has about 17~~.300.000 nodes~~*10^6~~, composed by~~ tetrahedral elements with a maximum edge size of 0.5 mm. Great attention should be given for the generation of the~~For the~~ mesh for the ~~fluid~~ lattice domain.~~,~~ Mesh accuracy and shape discretization should be balanced to find a profitable trade-off between reliable results and computation time. In addition, the mesh quality indexes (i.e. maximum aspect ratio) should be checked and minimized to guarantee a good convergence of the solution. Definitively, the setup of these parameters is not an easy task for the mesh of gyroid lattice and great effort has been put to obtain valuable results.

Moreover, the use of ~~it is important~~ $K-\omega\ SST$ model requires ~~to select the~~ the mesh refinement at the walls. A proper ~~*proper*~~ *near wall treatment method* is fundamental to~~to~~ solve accurately the boundary layer velocity profile and, consequently, to obtain~~ a~~ reliable prediction~~s~~ of the channel pressure drop. Two methos are investigated by considering the *castellation refinement* or the *inflation algorithm*~~ or the *castellation refinement*~~ [32] in order to obtain in both cases a maximum *y+* value lower than the unit at the wall.

The first method thickens the cell density uniformly in space near the outer walls while the second one creates stacked and elongated layers of cells near the walls, a comparison between the two mesh topologies is shown in Figure 11c-11d.

The castellation refinement reproduces the lattice geometry with great accuracy but it requires a huge computational effort. The resulting mesh is very heavy and it is prone to generate low quality cells and errors depending on little inaccuracies of the starting 3D geometry.

On the counterpart, the inflation algorithm has many advantages since it allows to~~ Even if the obtained *y+* values are similar, the first solution provides better counterpressure values, similar to the obtained experimental data of chapter 6, while the second one does not. A comparison between the two mesh topologies is shown in Figure 9c-9d. The first solution needs a simplification of the lattice geometry but it is chosen since it~~ drastically reduce~~s~~ the number of cells (-80% of elements), both reducing the computational resources and the time; and it~~,~~ favour~~ss~~ the numerical convergence of the solution~~ and guarantees more accurate results~~; whereas it requires a preliminary simplification of the lattice geometry. For example, it is clearly visible the smoothing of the sharp edges in Figure 11c. This finding is very important and it is proven to have predominant effect on

ha formattato: Tipo di carattere: Non Grassetto

ha formattato: Apice

ha formattato: Non Evidenziato

ha formattato: Tipo di carattere: Corsivo

ha formattato: Tipo di carattere: Corsivo

ha formattato: Tipo di carattere: Non Grassetto

ha formattato: Tipo di carattere: Non Grassetto

Codice campo modificato

the solution results, as broadly discussed in Section 7. The main reason found is that the relative density of the lattice is slightly increased of (+1; +1.5%) and the computed counterpressure is highly sensitive to this changing. After many attempts, the *inflation algorithm* is chosen for the mesh, making sure to check again the relative density of the meshed component. A summary of the main advantages and drawbacks of each technique is shown in Table 6.

ha formattato: Non Evidenziato

ha formattato: Tipo di carattere: Non Corsivo

ha formattato: Tipo di carattere: Non Grassetto

Codice campo modificato

(a)

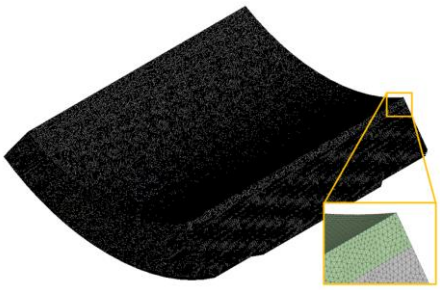

(b)

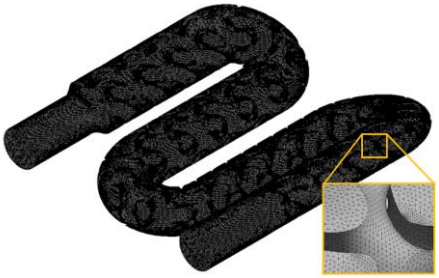

(c)

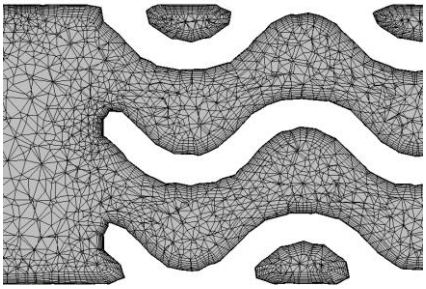

(d)

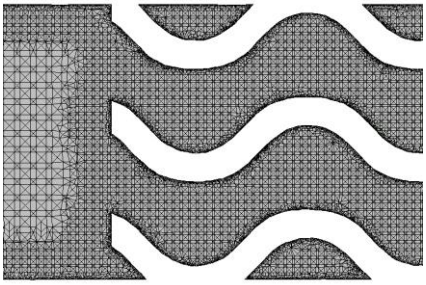

***Figure ~~11~~ 11~~9~~**. CFD space discretization: **a)** mesh of solid domain; **(b)** mesh of fluid domain; **(c)** inflation refinement at wall; **(d)** castellation refinement at wall.*

Table 6. *Pros and cons comparison of near wall treatment methods.*

		Castellation algorithm		***Inflation algorithm***
Computational effects	✘	Resources onerous	✓	Coarser mesh
	✘	Time expensive	✓	Faster computation
	✘	Prone to errors	✓	Better convergence
Geometrical effects	✓	Wall $y+ < 1$	✓	Wall $y+ < 1$
	✓	Accurate reconstruction	✘	RD error (1-1.5%)
	✘	Low cell quality	✓	Good cell quality

Finally, a mesh sensitivity analysis is performed by increasing the number of cells till there are no more changes in the computed variables of interest, i.e. the pressure drop. For the analysis the most critical condition is considered: pad "sheet 35%", water as coolant at the maximum flow rate for the application (6L/min).

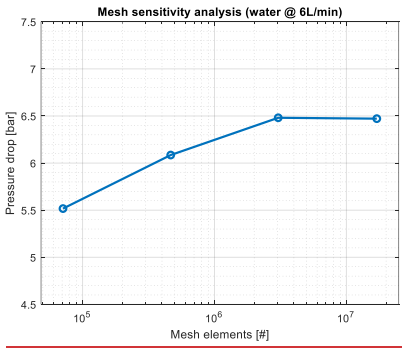

Figure 12*. Mesh sensitivity analysis on cell number for pad "sheet 35%".*

Tabella formattata

ha formattato: Tipo di carattere: Corsivo

ha formattato: Tipo di carattere: Corsivo

Formattato: Allineato al centro

ha formattato: Tipo di carattere: (Predefinito) Calibri, 11 pt, Colore carattere: Automatico

Formattato: Normale, SpazioPrima: 0 pt

5.3 Boundary conditions

For the setup of the simulation, the following boundary conditions (BCs) have been assumed, as shown in Figure 13~~Figure 13~~~~Figure 10~~. Actually, they are derived from the existing literature for the thermal analysis of lattices and they mimic the experimental conditions. Namely, flow rate and temperature are imposed at the inlet for the coolant, while the outlet is considered isobaric with the atmospheric pressure. The convection with oil is imposed on all the outer walls, that are effectively wetted by the lubricant oil in the real bearing. The biggest~~Actually, they allow easy comparisons of the thermal performances, even if they introduce a~~ simplification is introduced for the *sliding surface* temperature distribution, which is modelled as constant to reduce the model complexity. The value is the mean temperature approximated from Figure 3c. The ~~choice~~stability of the BCs is checked by applying slight changes to prove the stability of the model, finally they are considered reliable for the analysis.

A recap of the applied boundary conditions is reported below:

- Inlet — Flow normal velocity~~:~~, 40°C
- Outlet — Atmospheric pressure
- Sliding surface — Imposed temperature~~:~~, 60°C
- Other walls — Convection with oil at 50°C, $h = 50\ {}^{W}/_{m^2 \cdot K}$

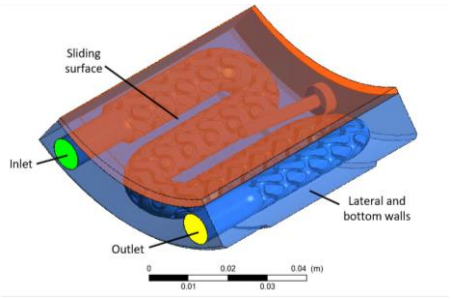

Figure ~~13~~~~13~~~~10~~. *Boundary conditions for CFD simulation setup.*

~~5.2~~5.4 CFD results analysis

The results of the CFD analysis are listed in Table 7~~Table 7~~~~Table 5~~ for a fluid flow rate of 6L/min, where the thermo-fluid dynamic properties are quantified in terms of pressure drop in the channel and heat exchange, between the solid part and the coolant. The baseline solution and

ha formattato: Tipo di carattere: Non Grassetto

ha formattato: Tipo di carattere: Non Grassetto, Colore carattere: Automatico

ha formattato: Tipo di carattere: Non Grassetto, Non Corsivo, Colore carattere: Automatico, Controllo ortografia e grammatica

Formattato: Rientro: Prima riga: 0 cm

ha formattato: Tipo di carattere: Non Grassetto, Colore carattere: Automatico

gyroid “sheet 35%” lattice are compared, for different fluids (water and oil ISOVG68) and solid materials (SS316L steel and copper).

Table 7~~5~~. *CFD material analysis for fluid flow rate of 6L/min.*

Internal Layout	***Fluid material***	***Solid material***	***Pressure drop [bar]***	***Exchanged heat [W]***
6-channels	Oil ISOVG68	SS316L	0.983	160
	Water	SS316L	0.121	248
	Water	Copper	0.121	877
Sheet 35%	Oil ISOVG68	SS316L	~~9.294~~10.071	212
	Water	SS316L	2.884	373
	Water	Copper	2.884	1120

ha formattato: Tipo di carattere: Grassetto

Tabella formattata

ha formattato: Tipo di carattere: Grassetto

ha formattato: Tipo di carattere: Grassetto

First of all, it is important to compare the cooling power values with respect the estimation of the heat production, due to frictional losses. From the TEHD model of the baseline solution, power loss is about 600 W on the bottom pad, so gyroid lattice can extract a significant quantity of the generated heat. When water and copper are used, the cooling power seems to be higher than the heat production rate: actually, this is a consequence of the ~~isothermal~~ fix-temperature boundary condition assumed for the sliding surface, useful for the following comparative analysis but not accurate in representing the real case.

When oil is used as coolant, no significant advantages can be highlighted for the steel pad, probably because the excessive coolant viscosity limits the beneficial effect of vorticity imposed by the lattice. For the “sheet 35%” lattice, a rather high pressure drop of approximately ~~9~~10 bar is obtained. Conversely, the improvements are notable when using water ~~and~~and gyroid lattice increases the heat exchange ~~increases~~ considerably up to~~of~~ +50.4~~0~~%, with respect to the baseline 6-channels pad. ~~.~~

Finally, the use of copper is a promising solution and it would increase the performances of gyroid lattice when coupled with water as coolant. It is here proposed only ~~in terms of~~referring to the thermal properties, while the mechanical properties are preliminary checked and they are compatible with the application. By using copper, pressure drop remains the same while ~~6-channels geometry increases~~the exchanged heat increases by +200~~448~~% ~~and gyroid by +600%~~both for 6-channels and gyroid lattice ~~with respect~~compared to the respective geometries~~y~~ made of steel.

Further studies and tests ~~will be performed~~are required with a copper alloy suitable for BMD process.

Moreover, it is interesting to consider the flowing regime by using the *Turbulent Intensity (TI)* as a convenient indicator [33]; usually it ranges between 0% (laminar flow) and 30% (fully turbulent flow). Reynolds number is not used, because it is difficult to define the reference dimensions for a complex structure such as gyroid lattice. In the simulations, a typical value of TI=5% is imposed at fluid inlet (common choice to mimic the fluid flowing in a straight pipe) and the same parameter is checked at lattice outlet. From the results, oil reaches a TI≈0% in the cooling circuit, therefore flow regime is purely laminar and heat convection is controlled by the large eddies of the coolant, imposed by the lattice; while water reaches the turbulent regime (TI≈20%), which guarantees a remarkable increasing of the effective heat transfer rate.

The pressure fields for the baseline and "sheet 35%" pads are shown in Figure 14~~Figure 14~~~~Figure 11~~, when oil is used as coolant, whereas the temperature distributions are shown in Figure 15~~Figure 15~~~~Figure 12~~ for the water case. The sections are chosen to be the best representative for the corresponding shown variable.

ha formattato: Tipo di carattere: Non Grassetto

Formattato: Rientro: Prima riga: 0 cm

ha formattato: Tipo di carattere: Non Grassetto

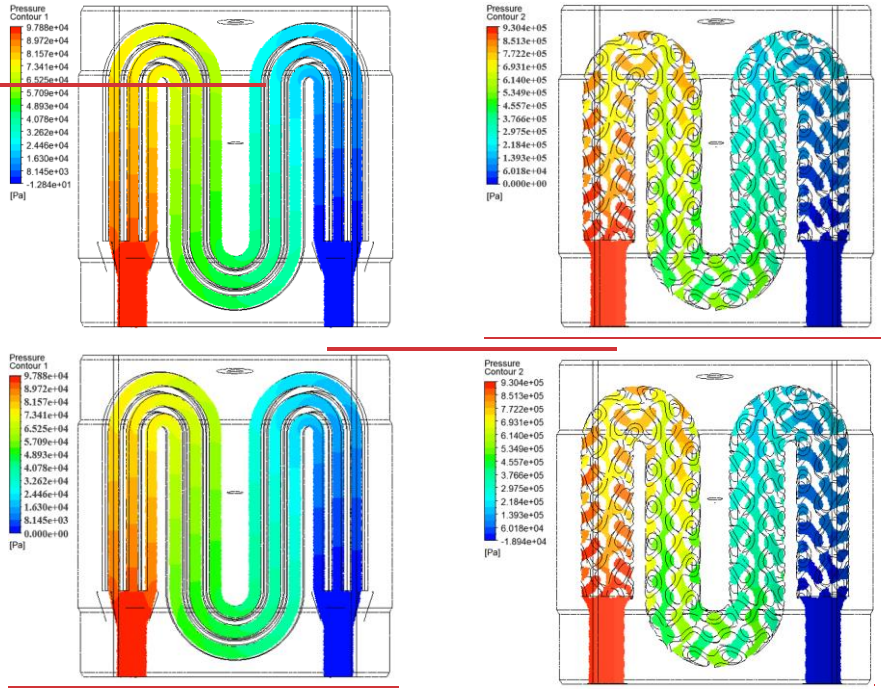

(a) (b)

Figure 14~~11~~. *CFD analysis, comparison of pressure field on meridian cross section, oil ISOVG68, 6L/min:* ***(a)*** *baseline 6-channels,* ***(b)*** *"sheet 35%" lattice.*

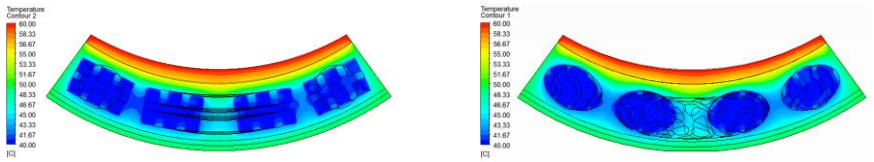

(a) (b)

Figure 15~~12~~. *CFD analysis, comparisons of temperature distribution on transversal cross section, water, 6L/min:* ***(a)*** *baseline 6-channels,* ***(b)*** *"sheet 35%" lattice.*

It is also notable to consider the effect of flow rate on the two geometries. This comparison is the most effective, because the gyroid lattice base concept is to induce the fluid turbulence. The pressure drop ΔP and the heat exchange Q as a function of the coolant flow rate are shown in Figure 16~~Figure 16~~~~Figure 13~~ and Figure 17~~Figure 17~~~~Figure 14~~ respectively, for the baseline 6-

ha formattato: Tipo di carattere: Non Grassetto, Non Corsivo

ha formattato: Tipo di carattere: Non Grassetto, Colore carattere: Automatico

channels pad and for “sheet 35%” layouts, both in the case of oil and water as coolant. The maximum flow rate for the application is considered to be 6L/min and a flow rate of 12L/min ~~Looking~~is computed only to compare the trend lines. Looking at the pressure curves, the behaviour is similar for the two coolants, but considerably higher pressures values are required for the oil case, just depending on its higher viscosity than the water. However, the exchanged heat trend is different for the two coolants. In the case of oil the flow regime is laminar, both in 6-channels and gyroid layout, so the curve shape is similar and simply shifted upward, due to the higher wetted surface of gyroid channel. Conversely, when the water is considered, the flow regime becomes turbulent in the gyroid channel and the heat exchanged can be relevantly increased. Therefore, gyroid heat exchange performances are clearly favourable, when turbulence occurs and the advantage between the two geometries increases for higher coolant flow rate.

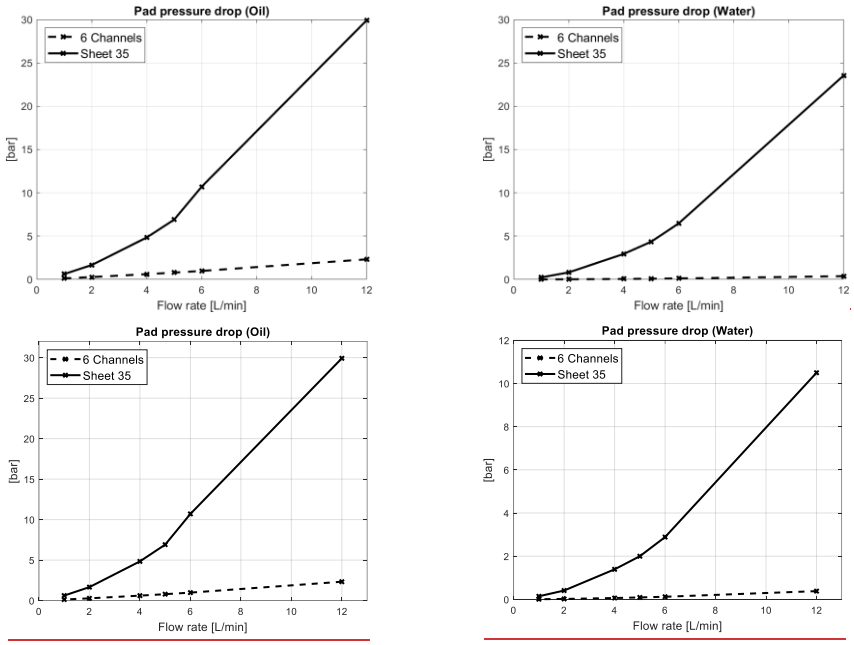

(a) (b)

Figure ~~16~~16~~13~~. *CFD pressure drop comparison as a function of flow rate for the two geometries by using oil* ***(a)*** *and water* ***(b)*** *as coolant.*

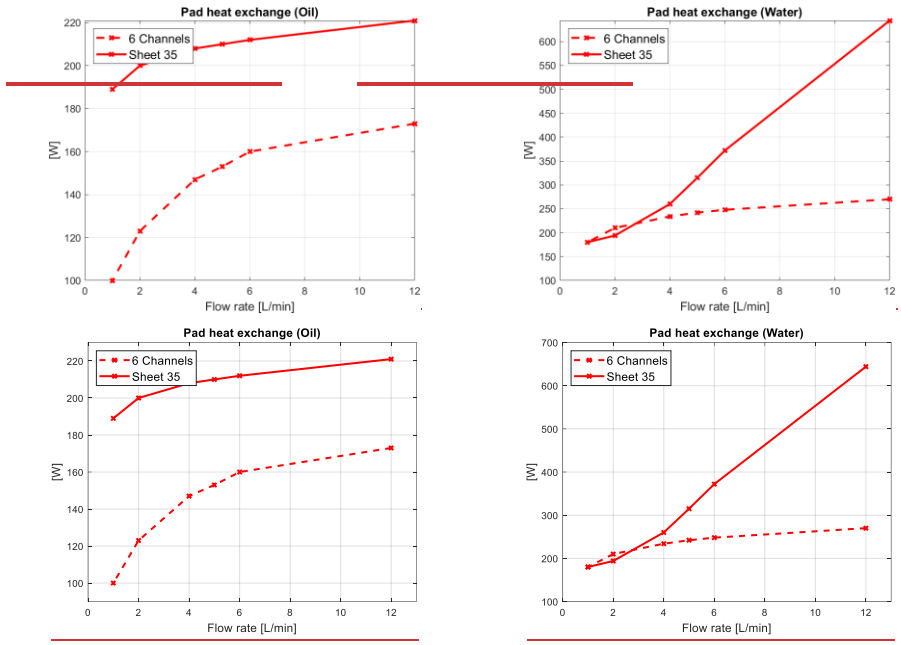

(a) (b)

***Figure 17~~17~~14**. CFD heat exchange comparison as a function of flow rate for the two geometries, by using oil **(a)** and water **(b)** as coolant.*

Formattato: Didascalia, Allineato a sinistra, SpazioPrima: 6 pt, Interlinea: singola

6 Experimental flushing test

6.1 Experimental setup

The experimental campaign is carried out to validate the pressure drop values of the numerical model with oil ISOVG68 and water. The experimental setup is mainly composed of two subassemblies, the hydraulic system and the flushing circuit. The external hydraulic system has been used to provide pumping pressure and to keep the oil temperature at 40±1~~0.5~~ °C by means of a temperature controller. The oil viscosity (and the directly related pressure drop) is very sensitive to the temperature. The oil inlet temperature value is chosen as a reference, because it is a significant operation parameter for the cooled pad.

When water is used, the pumping arrangement is substituted by a pressurized circuit with water at ambient temperature (17 °C); note that temperature control is no more significant in this case.

Formattato: Rientro: Prima riga: 0 cm

The flushing circuit is shown in Figure 18~~Figure 18~~Figure 15~~a~~, where the coolant flows from the left to the right passing through a temperature probe and reaching a crossroad regulated by two

ha formattato: Tipo di carattere: Non Grassetto

manual valves. The lower branch is used for the recirculation of the oil during the start-up procedure, allowing the thermal regime to be achieved, before starting with measurements, while it is not used for water. Right branch contains a pressure probe immediately before the pad sample, while the lattice outlet port can be considered isobaric with the ambient pressure. The fluid flow rate is adjusted with a regulating valve on the hydraulic system and then checked by weighting out the coolant flowed in a certain time interval with a scale.

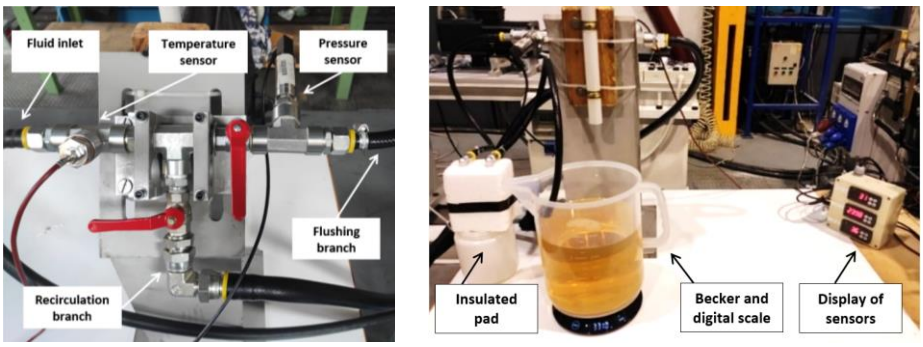

(a) (b)

Figure ~~18~~18~~15~~. Flushing hydraulic circuit (a) and measuring set up (b).

The measuring set-up is shown in Figure 18~~Figure 18~~~~Figure 15~~b, with the insulated pad on the left and a becker for fluid weighting on the digital scale. The pad is insulated with a thermal protection in polystyrene to keep it at desired temperature. The nominal flow rate is ranged from 1L/min to 6L/min, by acting on the regulating valve of the hydraulic system, but flow rates higher than 3L/min are not reachable for the oil, because they require an excessive hydraulic head for the pump; a similar issue occurs also for the water. Since connecting tubes have quite small diameter, their pressure drop can be significant, so they are flushed separately, by connecting them in series, to consider their pressure drop contribution.

Since flow rate is not closed loop controlled, operating conditions are checked for each measurement: the pressure and the temperature are measured by sensors, while the flow rate is calculated and adjusted. The measures are performed on the two printed pads, both with oil and water. They are repeated five times for robustness and uncertainty analysis is performed. The average error on flow rate is ±0.3%, while sensitivity for pressure is ±2mbar and for temperature is

ha formattato: Tipo di carattere: (Predefinito) Calibri, 11 pt, Colore carattere: Automatico

Formattato: Normale, SpazioPrima: 0 pt

ha formattato: Tipo di carattere: Non Grassetto

±~~0.015~~1 °C. All the measuring uncertainties are considered acceptable for the characterization of the pad.

6.2 Experimental results analysis

The resulting resistance curve (pressure versus flow rate) is obtained with a 2-order polynomial regression. For the mathematical model, zero-order term is imposed null to reflect physics of the problem, the confidence and the prediction intervals are plotted with a confidence level of 95% ~~and the correlation coefficient is determined~~. The measures figure out a high repeatability, as proved by the high values of the computed Correlation coefficient (*R-Sq*), around 99%; then no disturbance effects have arisen when experiments are performed. During the oil flushing, the temperature fluctuations have been the most critical variable to be controlled because of the external environmental disturbances, nevertheless a fine tuning of the set-up was sufficient to keep the oil temperature constant, obtaining low influences on the measures. The resulting pressure curves for the pad #1~~2~~ are reported in Figure 19~~Figure 19Figure 16a 16b~~, for both oil and water, while results for pad #2 are shown in Figure 20. ~~;~~ By looking at the data, it is noteworthy to consider that pad #2 requires a higher counterpressure (approximately +23.6% with oil and +14.7% with water) than pad #1 at the same operating conditions. Since the nominal geometry is equal, the differences can be addressed only to the change in the layering orientation, and so, to the surface roughness and to the printing accuracy of the internal channels.

ha formattato: Tipo di carattere: Non Corsivo, Non Apice / Pedice

ha formattato: Tipo di carattere: Non Corsivo

ha formattato: Tipo di carattere: Non Corsivo

ha formattato: Tipo di carattere: Non Corsivo

ha formattato: Tipo di carattere: Non Corsivo

ha formattato: Non Evidenziato

ha formattato: Tipo di carattere: Non Grassetto

ha formattato: Non Evidenziato

ha formattato: Non Evidenziato

ha formattato: Non Evidenziato

ha formattato: Tipo di carattere: Non Corsivo

ha formattato: Tipo di carattere: Non Corsivo

ha formattato: Tipo di carattere: Corsivo

Formattato: Rientro: Prima riga: 0 cm

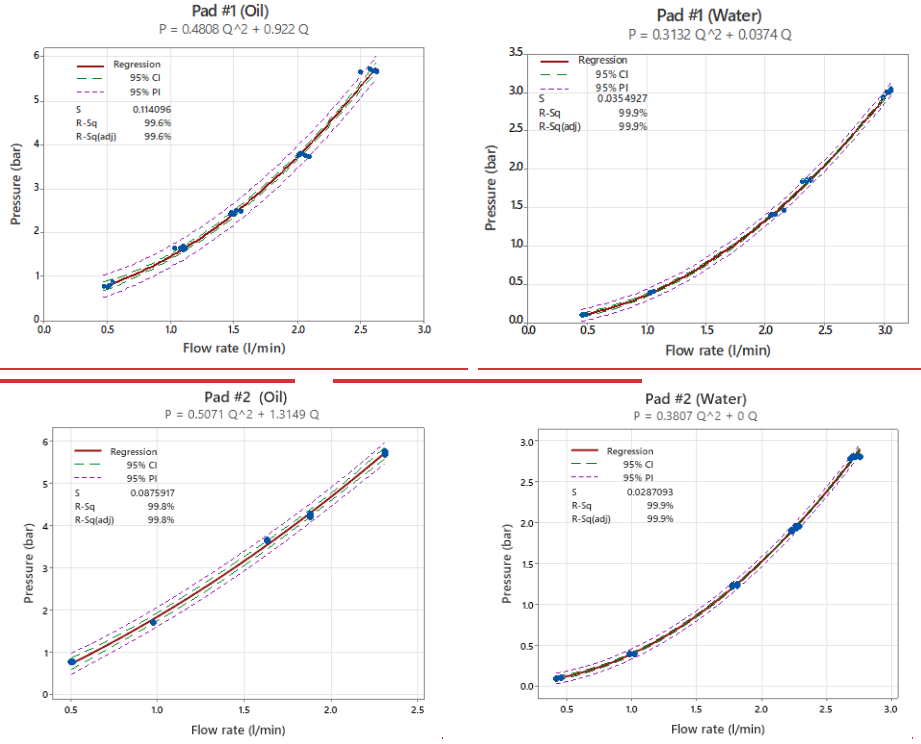

(a)~~(a)~~ (b)~~(b)~~

***Figure 19~~19~~16**. Experimental pressure curve for pad #~~2~~1 in oil **(a)** and water **(b)** measured with tubes.*

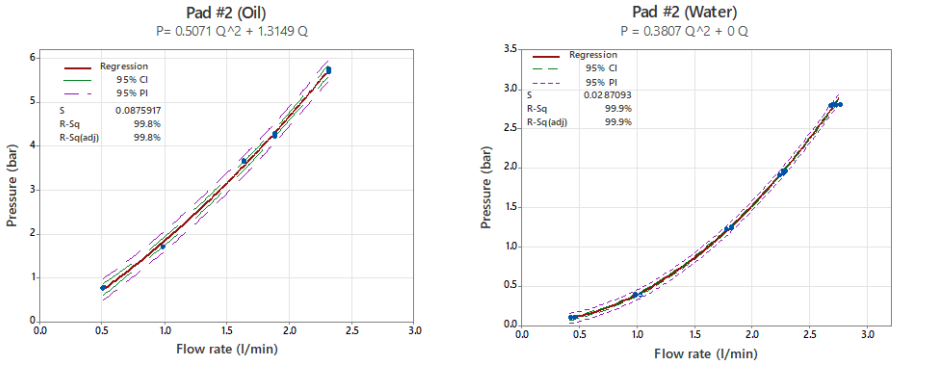

(a) (b)

***Figure 20~~20~~**. Experimental pressure curve for pad #2 in oil **(a)** and water **(b)** measured with tubes.*

Finally, experimental flushing has been performed also on 6-channels pad. Even though this prototype comes from some previous research activities, there were no reliable measures of its experimental counterpressure. These quantities are interesting to validate the numerical model of the baseline solution, so it has been flushed in the same manner of the other pads. The resulting pressure curves are shown in Figure 21.

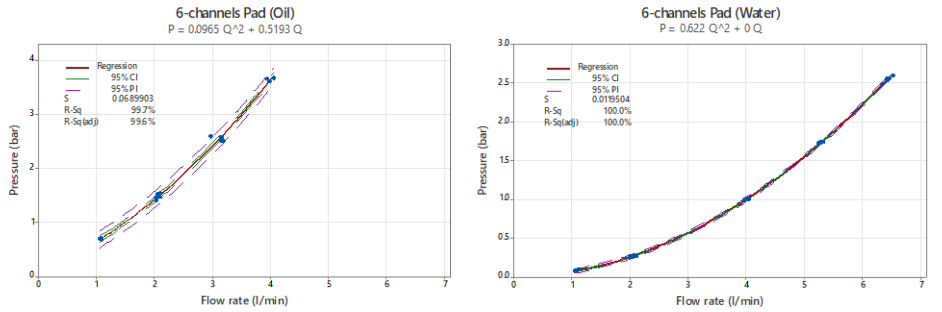

(a) (b)

***Figure 21**. Experimental pressure curve for 6-channels pad in oil **(a)** and water **(b)** measured with tubes.*

7 Comparison between CFD simulation and experimental results

The experimental results of pressure data are used to properly tune the numerical model, by considering the flushing of the two pads both with oil and water as coolant. In order to quantify the differences in an accurate way, interpolating polynomials are calculated from raw data and then used to estimate the pressure curves at nominal flow rates from 1L/min to 3L/min. The pressure drop related to the connecting tubes is subtracted ~~and the error is calculated as pressure difference~~and the comparison between numerical and experimental pressure curves ~~(CFD-Experimental),~~is ~~as~~ shown in Figure 22~~Figure 22Figure 17a-17b~~. By looking at the results for the gyroid pad, the numerical model with the nominal geometry (sheet RD=35%) ~~and the smooth wall~~ relevantly~~s~~ underestimates the experimental values. ~~with a percentual difference around -31% for oil and -20% for water.~~ Moreover, the pressure error increases with flow rate in both cases. The difference between pad #1 and pad #2 is ~~notew~~evident and it related to the lower printing accuracy

ha formattato: Tipo di carattere: (Predefinito) Calibri, 11 pt, Corsivo, Colore carattere: Automatico

Formattato: Normale, Allineato al centro, SpazioPrima: 0 pt

Formattato: Didascalia, Giustificato, SpazioPrima: 6 pt, Interlinea: 1.5 righe

ha formattato: Tipo di carattere: Non Corsivo, Colore carattere: Nero

ha formattato: Tipo di carattere: (Predefinito) +Corpo (Calibri), 12 pt, Non Corsivo, Colore carattere: Nero

ha formattato: Tipo di carattere: Non Corsivo, Colore carattere: Nero

ha formattato: Tipo di carattere: (Predefinito) +Corpo (Calibri), 12 pt, Non Corsivo, Colore carattere: Nero

ha formattato: Tipo di carattere: Non Corsivo, Colore carattere: Nero

ha formattato: Tipo di carattere: (Predefinito) +Corpo (Calibri), 12 pt, Non Corsivo, Colore carattere: Nero

ha formattato: Tipo di carattere: Non Corsivo, Colore carattere: Nero

ha formattato: Tipo di carattere: (Predefinito) +Corpo (Calibri), 12 pt, Non Corsivo, Colore carattere: Nero

ha formattato: Tipo di carattere: Non Corsivo, Colore carattere: Nero

ha formattato: Tipo di carattere: (Predefinito) +Corpo (Calibri), 12 pt, Colore carattere: Nero

ha formattato: Tipo di carattere: Corsivo

ha formattato: Tipo di carattere: Corsivo

Codice campo modificato

ha formattato: Tipo di carattere: Corsivo

ha formattato: Tipo di carattere: (Predefinito) +Corpo (Calibri), 12 pt, Corsivo, Colore carattere: Nero

Formattato: Allineato al centro, SpazioDopo: 8 pt, Interlinea: singola, Non sillabare, Regola lo spazio tra testo asiatico e in alfabeto latino

ha formattato: Tipo di carattere: Non Grassetto, Non Corsivo

measured on pad #2, as already mentioned in Section 6.2~~orthy and it can be related to the surface roughness and to the printing accuracy of the internal channels, depending on the layering orientation~~. When looking at 6-channels pad, the pressure error is ~~lower (around 9%)~~less significant and it is almost constant with respect to flow rate, probably because of the easier shape of the channels and the different AM process used (Selective Laser Melting). The comparison between the numerical and the experimental results clearly show a lack in the numerical model that is strictly related to the manufacturing technique of the prototypes.

Formattato: Rientro: Prima riga: 0 cm

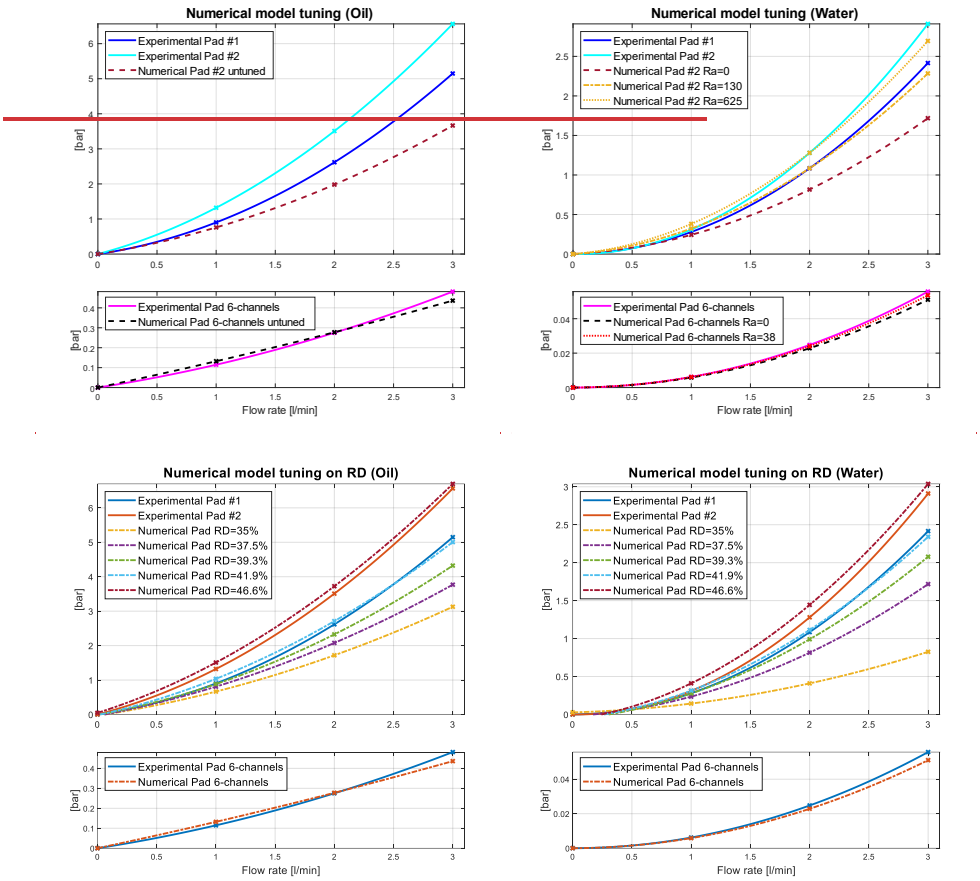

(a) (b)

Figure 22~~21~~7. *Pressure curves for pad #1, pad #2 and 6-channels; tuning of CFD model for Relative density in oil* ***(a)*** *and water* ***(b)****.*

Formattato: Allineato al centro, Rientro: Prima riga: 0 cm

As discussed by Hartsfield et al. in [34], the estimation of flow characteristics of AM parts, like the pressure drop, is still cumbersome. The numerical model should take into account for local and generalized printing defects and the layering effect on the surface roughness, which are difficult to estimate *a priori* because they depend on the geometry and the printing setup parameters~~setu.p. Moreover, common CFD codes use a sand-grain roughness model, which is not suitable for AM parts, so an equivalent average roughness value Ra_{eq} should be defined. This parameter differs from~~

~~the measured one and the comparative relations just start to be present in the literature [35]. They mostly depend on the AM process and BMD technology has not been studied yet on this matter. From the literature, the equivalent roughness is higher than the Ra parameter and it can be obtained by the product with a corrective factor as:~~

~~$$Ra_{eq} = Ra_{measured} * K_{printing\ setup} \quad (2)$$~~

The authors here propose a preliminary investigation of this topic, by performing a qualitative geometrical check on the printed geometry. A reasonable explanation of the pressure differences depends on three main aspects:

- Macroscopic printing errors;~~,~~
- Actual relative density;
-
- Wall roughness~~.~~;
- ~~Actual relative density~~

The first aspect can be caused, for example, by incorrect nozzle deposition in green parts or anisotropic shrinkage, which give rise to localized pressure losses. The internal geometry of pad #2 ~~channels~~ is inspected by means of *Computed tomography* (X-Ray CT) scans. The results are attached to this paper as MP4 videos in the supplementary material. Some localized dross formation and filament detachment are noticed, in particular near overhang regions, as shown in Figure 23 ~~Figure 18a~~. These errors are interesting but difficult to be modelled in the numerical analysis. Unfortunately it is not possible to perform reliable calculations to measure the printed relative density because of an insufficient scanning accuracy. ~~The scans have been also used to measure the real volume of the printed lattice, namely the relative density. Due to the scan accuracy, this calculation is difficult to be done on the pad but it is performed on "sheet 35%" cylindrical tube, as shown in Figure 18b. Actually, the relative density is found to be equal to 39.7%, higher than the nominal one (35%), therefore the channels cross section available for the coolant will be lower, resulting in a higher pressure drop.~~Anyway, it is certain that the presence of diffused printing defects affects in a negative way the fluid dynamic performances of the cooling channel. This~~ese~~ can be ~~some~~ a reasonable justification for the measured pressure differences, both for the oil and water case and it will be discussed in this section. ~~.~~

ha formattato: Non Evidenziato

Formattato: Giustificato, Rientro: Prima riga: 1.25 cm, SpazioPrima: 0 pt, Dopo: 0 pt, Sillabare, Non regolare lo spazio tra testo asiatico e in alfabeto latino

ha formattato: Tipo di carattere: (Predefinito) +Corpo (Calibri), 12 pt

ha formattato: Tipo di carattere: Non Grassetto, Non Corsivo

Codice campo modificato

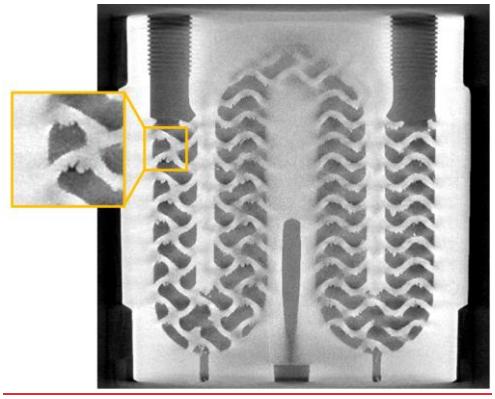

Figure 23~~2318~~. *X-Ray CT scan~~s~~ of the printed ~~parts: (a)~~ pad #2, meridian section.~~, (b) cylindrical sample.~~*

~~The second important parameter to be considered is the~~Finally, the surface roughness parameter has to be considered.~~ ~~Even though this indicator is very sensitive to the layering choice and so to the printing accuracy, actually it is not convenient for a process of parametrical tuning. First of all, the ~~Even if the~~ measured roughness values are not ~~suitable~~ useful for the CFD codes because they use a sand-grain roughness model. Unfortunately this is not suitable for AM parts because it neglects the important effects of oriented layering and directional roughness~~, they can be used as an indicator of the printing accuracy depending on the layering choice. Pad #~~ which are dominant for AM parts. Moreover, the wall roughness affects the counter pressure value only in turbulent regime (water coolant for the case study) but not in laminar regime when oil is used, as discussed in Section 5.1. Thereby, the roughness parameter is not effective for the tuning process.~~2 has almost a double roughness value than pad #1 and it can be a hint for lower printing accuracy. Only with water, the flow regime of the coolant is turbulent, so the numerical model can be tuned by changing the equivalent average roughness value. The relation between the roughness parameter and the percentual pressure increase for "sheet 35%" pad is shown in Figure 19.~~

Formattato: Allineato al centro

Formattato: Rientro: Prima riga: 0 cm

ha formattato: Non Evidenziato

ha formattato: Non Evidenziato

ha formattato: Non Evidenziato

ha formattato: Non Evidenziato

ha formattato: Non Evidenziato

ha formattato: Non Evidenziato

ha formattato: Non Evidenziato

ha formattato: Non Evidenziato

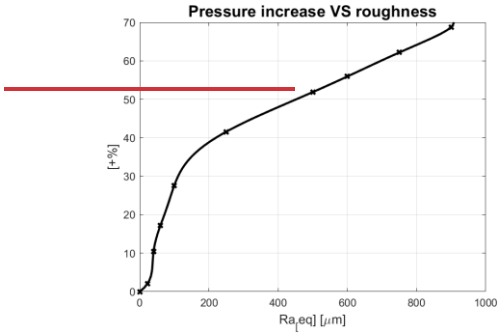

~~***Figure 19.*** *Sensitivity analysis of pressure increase as a function of roughness.*~~

As a consequence of the mentioned remarks, the tuning process of the

~~Finally, the~~ CFD model is ~~tuned~~ performed on the Relative Density (*RD*) parameter in order to ~~capture~~ reproduce the experimental pressure curves ~~in~~both in oil and ~~the~~ water case~~s~~. As already mentioned in Section 5.2, the pressure drops values estimated by the numerical model are highly sensitive to the relative density of the sheet lattice, this important outcome is exploited to correctly tune the numerical model.

A sensitivity analysis is performed by repeating the numerical simulations; all the boundary conditions and the setup procedure are kept the same and only the relative density of the lattice is increased step by step from 35% to approximately 45% (Figure 22). For this activity it is convenient to express the average increase of the pressure curve as percentage with respect to the numerical pressure curve calculated for pad with "sheet 35" lattice. For each simulation two values of density are given, before and after the meshing approximation for the Inflation algorithm, as discussed in the previous sections. This procedure assures a higher accuracy for the results because it takes into account the geometrical simplification given by the mesh. The computed pressure data both for oil and water are shown in Figure 24 and reported in a tabular way in Table 8.

ha formattato: Non Evidenziato
ha formattato: Non Evidenziato
ha formattato: Tipo di carattere: Corsivo
ha formattato: Non Evidenziato
ha formattato: Non Evidenziato
ha formattato: Non Evidenziato
ha formattato: Non Evidenziato
ha formattato: Tipo di carattere: Non Corsivo
ha formattato: Tipo di carattere: Non Grassetto, Non Corsivo
ha formattato: Non Evidenziato
Codice campo modificato
ha formattato: Non Evidenziato
ha formattato: Non Evidenziato
ha formattato: Non Evidenziato
ha formattato: Non Evidenziato
ha formattato: Non Evidenziato
ha formattato: Non Evidenziato
ha formattato: Non Evidenziato
ha formattato: Non Evidenziato
ha formattato: Non Evidenziato
ha formattato: Non Evidenziato
Formattato: Rientro: Prima riga: 1.25 cm, Sillabare, Non regolare lo spazio tra testo asiatico e in alfabeto

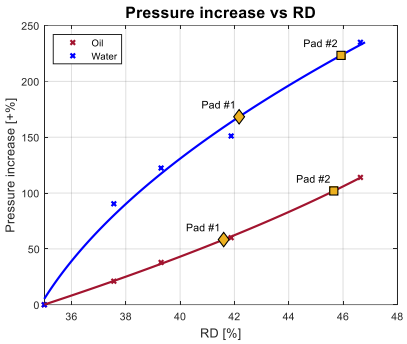

Figure 24. *Sensitivity analysis of pressure increase as a function of relative density (RD), numerical results.*

Table 8. *Tabular data of pressure increase as a function of relative density (RD).*

Relative Density (before meshing)	***Relative Density (after meshing)***	***Pressure increase (oil)***	***Pressure increase (water)***
35%	35.0%	+0%	+0%
35%	37.6%	+21%	+90%
37%	39.3%	+38%	+122%
40%	41.9%	+60%	+151%
45%	46.6%	+143%	+226%
Regression functions		$\Delta p_{oil} = 0.1816\ RD^2 - 5.09\ RD - 44.04$	
Validity range: $RD \in [35\%\,;47\%]$		$\Delta p_{water} = -0.8206\ RD^2 + 86.13\ RD - 2001$	

The graph shows the percentual increase of pressure by changing the relative density for the numerical model and the respective regression 2 order polynomial equations are calculated. The experimental regression lines for the correlation between the pressure increase and the relative density are reported in Table 8 and they become important for the design of the manufactured component. Both oil and water case are represented, moreover the experimental pressure values for pads #1 and #2 are reported as yellow markers of different shape. By inverting the computed equations and by applying them to the experimental pads, the required relative densities can be estimated. Pad #1 can be modelled with an equivalent numerical model with relative density around 42% while pad #2 around 46%. Please consider that these equivalent values of relative densities take into account all the inaccuracies of the manufacturing step and they may not correspond to

ha formattato: Tipo di carattere: Corsivo
ha formattato ...
ha formattato: Tipo di carattere: Corsivo
Formattato: Allineato al centro
ha formattato: Non Evidenziato
ha formattato ...
ha formattato: Tipo di carattere: Grassetto, Non Evidenziato
Tabella formattata
ha formattato ...
ha formattato ...
ha formattato: Non Evidenziato
ha formattato ...
ha formattato ...
ha formattato ...
ha formattato: Non Evidenziato
ha formattato ...
ha formattato ...
ha formattato ...
ha formattato: Non Evidenziato
ha formattato ...
ha formattato ...
ha formattato ...
ha formattato: Non Evidenziato
ha formattato ...
ha formattato ...
ha formattato ...
ha formattato: Non Evidenziato
ha formattato ...
ha formattato: Colore carattere: Automatico
ha formattato ...
ha formattato ...
Formattato ...
Formattato ...
ha formattato: Tipo di carattere: Grassetto
Formattato ...
ha formattato: Tipo di carattere: Grassetto
Formattato: Interlinea: multipla 1.15 ri
ha formattato: Non Evidenziato
ha formattato ...
ha formattato ...

the geometrical definition. This solution finds good agreement both for the oil and the water cases and the main results are summarized in Table 9.

Table 9. *Equivalent relative densities computed for the model tuning on pads.*

	Coolant type	***Pressure increase (oil)***	***Equivalent relative density***
Pad #1	oil	+58%	41.6%
	water	+168%	42.2%
Pad #2	oil	+102%	45.7%
	water	+223%	45.9%

~~. For pad #1 roughness parameter is chosen to be Ra_{eq}=130µm, while for pad #2 Ra_{eq}=625µm. These values include the error at the actual relative density of the gyroid. The oil tuning process on the roughness is not necessary, due to the laminar flow regime, and the pressure differences should be considered for the design phase. The pressure differences between the numerical model and the experimental data, are summarized in Table 6 along with the tuned equivalent roughness.~~

About the validity limits of the empirical equations is north worthy to state that they are suitable only for the current case of study, nevertheless the important aspect is the strong sensitivity of the pressure drop with respect to the relative density and this procedure can be easily reproduced for any other component. The most relevant outcome of the tuning process is that the printed lattices are featured by localized and diffused printing defects, which affects relevantly the counter pressure and they should be taken into account for the design of the component.

ha formattato: Tipo di carattere: Non Grassetto

Codice campo modificato

ha formattato: Tipo di carattere: Grassetto

Tabella formattata

ha formattato: Tipo di carattere: Grassetto

ha formattato: Tipo di carattere: Grassetto

ha formattato: Non Evidenziato

Formattato: Rientro: Prima riga: 0 cm

Table 6. Summary of experimental pressure error with respect to numerical model.

8 Pressure error		Smooth walls	Ra_{eq}
Oil ISOVG68	6 channels	7%	-
	Pad #1	20%	-
	Pad #2	43%	-
Water	6 channels	9%	38 µm
	Pad #1	16%	130 µm
	Pad #2	24%	625 µm

ha formattato: Tipo di carattere: (Predefinito) Calibri, 11 pt, Non Corsivo

Formattato: Allineato a sinistra, SpazioPrima: 0 pt, Dopo: 0 pt, Non mantenere con successivo

Formattato: Rientro: Prima riga: 1.25 cm

98 Conclusions

Bioinspired gyroid lattice is confirmed to be an effective solution for light-weighting of structural components and enhanced heat exchange. Static mechanical analysis and fluid dynamics properties have been deeply investigated in this paper by means of numerical simulations and experimental tests, to better understand the most suitable design set up for cooled pad in TPJB.

The application on TPJB has great opportunities of improvements: advanced internal cooling can reduce sliding surface temperature with beneficial effects on the bearing behaviour. In particular, for gyroid lattice, heat exchange can be increased at least of +50% with respect to the baseline solution. This investigation contributes to the worldwide trend to increase efficiency and performances of machines in engineering. More loaded pads, with the limit given only by the liner mechanical characteristics, allowcharacteristics, allow downsizing of oil film bearings, reducing the quantity of oil needed for lubrication and pushing this widely used technology to a more environmentally friendly level, especially if water is used for the internal cooling.

For further developments, a full Thermo-Elastic-Hydro-Dynamic model of the bearing could be implemented so that temperature distributions on pad surfaces are directly calculated at each iteration, leading to a more representative and reliable model of the bearing. Unfortunately, gyroid geometry is quite complicated and an efficient mesh solution becomes fundamental to avoid a too large computational effort in the CFD analysis.

The manufacturing of functional prototypes by means of Bound Metal Ddeposition is the key outcome of this research activity. Manufacturing setup have been tuned carefully to counterbalance

geometrical and dimensional defects. Moreover, the absence of excess metal powder inside the channels and easy printing of copper are relevant advantages of this technology.

Finally, comparisons between numerical and experimental data are useful to catch printing differences with the nominal geometry and to quantify the accuracy of the proposed numerical model.

Acknowledgments

The present work was undertaken under the support of the Italian Ministry for Education, University and Research by means of the project Department of Excellence LIS4.0 (Integrated Laboratory for Lightweight and Smart Structures).

References

[1] Stephen W, Giddings C, Lee S. Characterization of Hydrodynamic Lift Forces by Field-Flow Fractionation. Inertial and Near-Wall Lift Forces. Chem Eng Commun 1994;130:143–66.
[2] Kim S, Shin D, Palazzolo AB. A Review of Journal Bearing Induced Nonlinear Rotordynamic Vibrations. J Tribol 2021;143.
[3] Fillon M. Thermal and deformation effects on tilting-pad thrust and journal bearing performance, 2005.
[4] Dong Q, Yin Z, Li H, Gao G, Zhong N, Chen Y. Simulation and experimental verification of fatigue strength evaluation of journal bearing bush. Eng Fail Anal 2020;109:104275. https://doi.org/10.1016/j.engfailanal.2019.104275.
[5] Yang S, Kim C, Lee W. Prevention of fluttering fatigue damage in a tilting pad journal bearing. Tribol Int 2009;42:816–22.
[6] Mehdi SM, Jeong SY, Kim TH. Influence of Recess Dimensions and Jacking Oil Flow Rate on the Performance of Tilting Pad Journal Bearings with Jacking Oil Mechanism. Tribol Trans 2022;0:1–16.
[7] Cerda Varela A, Ferreira Santos I. Dynamic Coefficients of a Tilting Pad With Active Lubrication: Comparison Between Theoretical and Experimental Results. J Tribol 2015;137.
[8] Hagemann T, Schwarze H. Theoretical and Experimental Analyses of Directly Lubricated Tilting-Pad Journal Bearings With Leading Edge Groove. J Eng Gas Turbines Power 2018;141.
[9] Abdollahi B, San Andrés L. Improved Estimation of Bearing Pads' Inlet Temperature: A Model for Lubricant Mixing at Oil Feed Ports and Validation against Test Data. J Tribol 2018;141.
[10] Croné P, Almqvist A, Larsson R. Thermal Turbulent Flow in Leading Edge Grooved and Conventional Tilting Pad Journal Bearing Segments—A Comparative Study. Lubricants 2018;6:97.
[11] Varela AC, Santos IF. Component level study of an actively lubricated LEG Tilting Pad Bearing: Theory and experiment. Tribol Int 2018;120:115–26.
[12] Schüler E, Berner O. Improvement of Tilting-Pad Journal Bearing Operating Characteristics by Application of Eddy Grooves. Lubricants 2021;9:18.
[13] Yang J, Palazzolo A. Power loss reduction for tilt pad journal bearings utilizing pad pockets and steps. Tribol Int 2021.
[14] Najar FA, Harmain GA. Novel Approach Towards Thrust Bearing Pad Cooling, American Society of Mechanical Engineers Digital Collection; 2015.
[15] Najar F, Harmain G. Performance characteristics in hydrodynamic water cooled thrust bearings. J Tribol 2016;10:28–47.

ha formattato: Italiano (Italia)

[16] Chatterton S, Pennacchi P, Vania A, Dang PV. Cooled Pads for Tilting-Pad Journal Bearings. Lubricants 2019;7:92.
[17] Suh J, Palazzolo A. Three-Dimensional Dynamic Model of TEHD Tilting-Pad Journal Bearing—Part I: Theoretical Modeling. J Tribol 2015;137.
[18] Kaur I, Singh P. State-of-the-art in heat exchanger additive manufacturing. Int J Heat Mass Transf 2021;178:121600.
[19] Li W, Yu G, Yu Z. Bioinspired heat exchangers based on triply periodic minimal surfaces for supercritical CO2 cycles. Appl Therm Eng 2020;179:115686.
[20] Luo J-W, Chen L, Min T. Macroscopic transport properties of Gyroid structures based on pore-scale studies: Permeability, diffusivity and thermal conductivity. Int J Heat Mass Transf 2020;146:118837.
[21] Peng H, Gao F, Hu W. Design, modelling and characterization of Triply Periodic Minimal Surface heat exchangers with Additive Manufacturing, 2019.
[22] Michielsen K, Stavenga D g. Gyroid cuticular structures in butterfly wing scales: biological photonic crystals. J R Soc Interface 2008;5:85–94.
[23] Koneri R, Mulye S, Ananthakrishna K. Additive Manufacturing of Lattice Structures for Heat Transfer Enhancement in Pipe Flow. Ind. 40 Adv. Manuf., Singapore: Springer; 2021, p. 233–46.
[24] Zhang L, Feih S, Daynes S. Energy absorption characteristics of metallic triply periodic minimal surface sheet structures under compressive loading. Addit Manuf 2018;23:505–15.
[25] Al-Ketan O, Rezgui R, Rowshan R. Microarchitected Stretching-Dominated Mechanical Metamaterials with Minimal Surface Topologies. Adv Eng Mater 2018;20:1800029.
[26] Parenti P, Puccio D, Colosimo BM. A new solution for assessing the printability of 17-4 PH gyroids produced via extrusion-based metal AM. J Manuf Process 2022;74:557–72.
[27] 3D Printing: Desktop Metal Dimensional Accuracy & Surface Finish. Comput Aided Technol LLC 2022. https://www.cati.com/blog/2019/05/desktop-metal-dimensional-accuracy-surface-finish/.
[28] Dang PV, Chatterton S, Pennacchi P. The Effect of the Pivot Stiffness on the Performances of Five-Pad Tilting Pad Bearings. Lubricants 2019;7:61. https://doi.org/10.3390/lubricants7070061.
[29] Chatterton S, Pennacchi P, Dang PV, Vania A. A Test Rig for Evaluating Tilting-Pad Journal Bearing Characteristics. Mech Mach Sci 2015;21:921–30.
[30] Khaderi SN, Deshpande VS, Fleck NA. The stiffness and strength of the gyroid lattice. Int J Solids Struct 2014;51:3866–77.
[31] Petronas Arbor Hydraulic 68 ISO VG 68. Petronas Lubr Cat 2021. https://www.pli-petronas.com/it-it/agricoltura-e-macchine-movimento-terra/prodotto/petronas-arbor-hydraulic-68-iso-vg-68.
[32] Ferziger JH, Perić M. Computational Methods for Fluid Dynamics. Springer Berlin, Heidelberg; 2002.
[33] Marusic I, Kunkel GJ. Streamwise turbulence intensity formulation for flat-plate boundary layers. Phys Fluids 2003;15:2461–4.
[34] Hartsfield CR, Shelton TE, Cobb GR, Kemnitz RA, Weber J. Understanding Flow Characteristics in Metal Additive Manufacturing. J Aerosp Eng 2021;34:04021082.
~~[1] Stephen W, Giddings C, Lee S. Characterization of Hydrodynamic Lift Forces by Field-Flow Fractionation. Inertial and Near-Wall Lift Forces. Chem Eng Commun 1994;130:143–66.~~
~~[2] Kim S, Shin D, Palazzolo AB. A Review of Journal Bearing Induced Nonlinear Rotordynamic Vibrations. J Tribol 2021;143.~~
~~[3] Fillon M. Thermal and deformation effects on tilting-pad thrust and journal bearing performance, 2005.~~
~~[4] Dong Q, Yin Z, Li H, Gao G, Zhong N, Chen Y. Simulation and experimental verification of fatigue strength evaluation of journal bearing bush. Eng Fail Anal 2020;109:104275. https://doi.org/10.1016/j.engfailanal.2019.104275.~~
~~[5] Yang S, Kim C, Lee W. Prevention of fluttering fatigue damage in a tilting pad journal bearing. Tribol Int 2009;42:816–22.~~
~~[6] Mehdi SM, Jeong SY, Kim TH. Influence of Recess Dimensions and Jacking Oil Flow Rate on the Performance of Tilting Pad Journal Bearings with Jacking Oil Mechanism. Tribol Trans 2022;0:1–16.~~

[7] Cerda Varela A, Ferreira Santos I. Dynamic Coefficients of a Tilting Pad With Active Lubrication: Comparison Between Theoretical and Experimental Results. J Tribol 2015;137.
[8] Hagemann T, Schwarze H. Theoretical and Experimental Analyses of Directly Lubricated Tilting-Pad Journal Bearings With Leading Edge Groove. J Eng Gas Turbines Power 2018;141.
[9] Abdollahi B, San Andrés L. Improved Estimation of Bearing Pads' Inlet Temperature: A Model for Lubricant Mixing at Oil Feed Ports and Validation against Test Data. J Tribol 2018;141.
[10] Croné P, Almqvist A, Larsson R. Thermal Turbulent Flow in Leading Edge Grooved and Conventional Tilting Pad Journal Bearing Segments—A Comparative Study. Lubricants 2018;6:97.
[11] Varela AC, Santos IF. Component level study of an actively lubricated LEG Tilting Pad Bearing: Theory and experiment. Tribol Int 2018;120:115–26.
[12] Schüler E, Berner O. Improvement of Tilting-Pad Journal Bearing Operating Characteristics by Application of Eddy Grooves. Lubricants 2021;9:18.
[13] Yang J, Palazzolo A. Power loss reduction for tilt pad journal bearings utilizing pad pockets and steps. Tribol Int 2021.
[14] Najar FA, Harmain GA. Novel Approach Towards Thrust Bearing Pad Cooling, American Society of Mechanical Engineers Digital Collection; 2015.
[15] Najar F, Harmain G. Performance characteristics in hydrodynamic water cooled thrust bearings. J Tribol 2016;10:28–47.
[16] Chatterton S, Pennacchi P, Vania A, Dang PV. Cooled Pads for Tilting-Pad Journal Bearings. Lubricants 2019;7:92.
[17] Suh J, Palazzolo A. Three-Dimensional Dynamic Model of TEHD Tilting-Pad Journal Bearing—Part I: Theoretical Modeling. J Tribol 2015;137.
[18] Kaur I, Singh P. State-of-the-art in heat exchanger additive manufacturing. Int J Heat Mass Transf 2021;178:121600.
[19] Li W, Yu G, Yu Z. Bioinspired heat exchangers based on triply periodic minimal surfaces for supercritical CO2 cycles. Appl Therm Eng 2020;179:115686.
[20] Luo J-W, Chen L, Min T. Macroscopic transport properties of Gyroid structures based on pore-scale studies: Permeability, diffusivity and thermal conductivity. Int J Heat Mass Transf 2020;146:118837.
[21] Peng H, Gao F, Hu W. Design, modelling and characterization of Triply Periodic Minimal Surface heat exchangers with Additive Manufacturing, 2019.
[22] Michielsen K, Stavenga D g. Gyroid cuticular structures in butterfly wing scales: biological photonic crystals. J R Soc Interface 2008;5:85–94.
[23] Koneri R, Mulye S, Ananthakrishna K. Additive Manufacturing of Lattice Structures for Heat Transfer Enhancement in Pipe Flow. Ind. 40 Adv. Manuf., Singapore: Springer; 2021, p. 233–46.
[24] Zhang L, Feih S, Daynes S. Energy absorption characteristics of metallic triply periodic minimal surface sheet structures under compressive loading. Addit Manuf 2018;23:505–15.
[25] Al-Ketan O, Rezgui R, Rowshan R. Microarchitected Stretching-Dominated Mechanical Metamaterials with Minimal Surface Topologies. Adv Eng Mater 2018;20:1800029.
[26] Parenti P, Puccio D, Colosimo BM. A new solution for assessing the printability of 17-4 PH gyroids produced via extrusion-based metal AM. J Manuf Process 2022;74:557–72.
[27] 3D Printing: Desktop Metal Dimensional Accuracy & Surface Finish. Comput Aided Technol LLC 2022. https://www.cati.com/blog/2019/05/desktop-metal-dimensional-accuracy-surface-finish/.

[28] Dang PV, Chatterton S, Pennacchi P. The Effect of the Pivot Stiffness on the Performances of Five-Pad Tilting Pad Bearings. Lubricants 2019;7:61. https://doi.org/10.3390/lubricants7070061.
[29] Chatterton S, Pennacchi P, Dang PV, Vania A. A Test Rig for Evaluating Tilting-Pad Journal Bearing Characteristics. Mech Mach Sci 2015;21:921–30.
[30] Khaderi SN, Deshpande VS, Fleck NA. The stiffness and strength of the gyroid lattice. Int J Solids Struct 2014;51:3866–77.
[31] Petronas Arbor Hydraulic 68 ISO VG 68. Petronas Lubr Cat 2021. https://www.pli-petronas.com/it-it/agricoltura-e-macchine-movimento-terra/prodotto/petronas-arbor-hydraulic-68-iso-vg-68.
[32] Ferziger JH, Perić M. Computational Methods for Fluid Dynamics. Springer Berlin, Heidelberg; 2002.
[33] Marusic I, Kunkel GJ. Streamwise turbulence intensity formulation for flat-plate boundary layers. Phys Fluids 2003;15:2461–4.
[34] Hartsfield CR, Shelton TE, Cobb GR, Kemnitz RA, Weber J. Understanding Flow Characteristics in Metal Additive Manufacturing. J Aerosp Eng 2021;34:04021082.
[35] Shelton TE, Stelzer DJ, Hartsfield CR, Cobb GR, O'Hara RP, Tommila CD. Understanding surface roughness of additively manufactured nickel superalloy for space applications. Rapid Prototyp J 2020;26:557–65.